Spatial influence of agricultural~~e~~ residue burning and aerosols on land surface temperature

Akanksha Pandey[1], Richa Singh[1], Kumari Aditi[1,2], Neha Chhillar[1], Tirthankar Banerjee[1,2*]

[1] Institute of Environment and Sustainable Development, Banaras Hindu University, Varanasi, India.
[2]DST-Mahamana Centre of Excellence in Climate Change Research, Banaras Hindu University, Varanasi, India.
**Correspondence to*: T. Banerjee (tb.iesd@bhu.ac.in; tirthankaronline@gmail.com)

Abstract

The biophysical effects of agricultural ~~e~~ residue burning, driven by the excessive release of energy and carbonaceous aerosols, remain ~~largely unaccounted for~~poorly quantified at the global scale. Residue-based fires have the potential to modify regional climate by altering land surface temperature (LST), highlighting the need for investigation at regional scale. ~~based fire through excessive release of energy and carbonaceous aerosols essentially unaccounted globally. Elucidating climate feedback from residue-based fire however, remain pertinent as energy released from fire pose potential to modify land surface temperature (LST) thereby, regional climate.~~ Here, an observation-driven assessment of spatial ~~change~~ variations in LST due to concurrent release of energy and aerosols has been ~~explored~~ made over northwestern India using multiple satellite and reanalysis-based datasets. Year-specific fire pixel density was used to delineate an intensive fire zone characterized by medium-to-large residue-based fire. ~~Initially, year-specific fire pixel density was computed to identify intensive fire zone encompassing only medium to large fire.~~ Geos~~S~~patial analysis revealed positive ~~correlation~~ association among FRP (fire radiative power), LST and AOD (aerosol optical depth) ~~across the intensive fire zone~~. ~~Residue-based fire~~ Over intensive fire zone, a space-for-time approach revealed ~~accounted an increase in LST by 0.48°C and AOD by 0.19 yearly during peak fire season over intensive fire zone.~~ significant increase in both ΔLST (0.57°C; 95% CI:0.33-0.81°C) and ΔAOD (0.13; 95% CI:0.08–0.17) due to fire. ~~A~~ Random Forest non-linear model was employed to regress potential influence of FRP and AOD on LST having several other variables as confounding factors. FRP consistently emerged as the dominant predictor of LST, followed by planetary boundary layer height and aerosols. ~~Random Forest non-linear model was used to regress potential influence of FRP and AOD on LST across. Ttwo pre-constructed defined scenarios were evaluated to ascertain FRP-AOD-LST nexus. Interestingly, both scenarios recognized FRP remained as a top dominant predictor to influence LST in both the scenarios,~~

Formatted: Font color: Text 1

Formatted: Font color: Text 1

Formatted: Font color: Text 1

Formatted: Font color: Text 1

Formatted: Font color: Text 1

~~followed by solar radiation and AOD.~~ An increase ~~significant enhancement~~ in relative feature importance of FRP was ~~also~~ noted during days having high fire intensity and positive association ~~against~~ with LST. Geographically w~~W~~eighted ~~R~~regression further explained spatial heterogeneity in LST modulation by FRP. Overall, this analysis provides the first empirical evidence~~Our analysis therefore, provides first empirical evidence~~ that ~~on crop~~ residue-based fire ~~on~~ contributes to changes in ~~modifying regional climate by altering~~ land surface temperature. It further highlights that the magnitude of this perturbation is governed by interannual variations in fire intensity and influenced strongly by prevailing meteorological conditions. ~~It also underlines that extent of such perturbation is subject to year-specific fire intensity and govern by meteorology.~~

Formatted: Font color: Auto

Keywords: Aerosols, Biomass burning, Fire, GWR, Random Forest.

Introduction

Burning agricultural residues is a widespread practice for the rapid removal of post-harvest biomass from croplands in many regions of the world (Streets et al., 2003; Singh et al., 2018; Shyamsundar et al., 2019). While biomass burning is often associated with deforestation (Chuvieco et al., 2021), forest fires (van der Velde et al., 2021; Aditi et al., 2025), and shifting cultivation (Prasad et al., 2000), residue burning on agricultural land is primarily conducted to clear fields, fertilize soil, eradicate weeds and pests, and prepare land for the next crop cycle (Graham et al., 2002; Korontzi et al., 2006; Lan et al., 2022). This practice is observed across large agricultural regions globally, including China (Streets et al., 2003; Zhang et al., 2020), South America (Graham et al., 2002), Southeast Asia (Lasko and Vadrevu, 2018; Yin, 2020), and northwestern India (Singh et al., 2018, 2021; Sarkar et al., 2018). In northwestern India, extensive residue burning during October to November is a recurring phenomenon and has been widely examined from multiple perspectives. Previous studies report that these burning events contribute to severe air-quality degradation in downwind urban centers (Singh et al., 2018; Jethva et al., 2019), alter aerosol loading and chemistry (Mhawish et al., 2022), modify aerosol vertical stratification and radiative forcing (Hsu et al., 2003; Vinjamuri et al., 2020; Banerjee et al., 2021), induce adverse health effects (Singh et al.,

Formatted: Font color: Text 1

Formatted: Font color: Text 1

Formatted: Font: 9 pt

2021), and may influence regional hydrological processes (Kant et al., 2023). ~~Burning agricultur~~al~~e residues is a widespread practice for quick removal of post-harvest crop leftover from the field over many parts of the world (Streets et al., 2003; Singh et al., 2018; Shyamsundar et al., 2019). While burning biomass is often associated with the practice of deforestation (Chuvieco et al., 2021), forest fire (van der Velde et al., 2021; Aditi et al., 2025) and shifting cultivation (Prasad et al., 2000); agricultur~~al~~e residue burning is more commonly associated with cleaning farmland, fertilizing soil, eradicating pests and weeds, and making land suitable for the subsequent crop (Graham et al., 2002; Korontzi et al., 2006; Lan et al., 2022). Agriculture~~al~~ residue burning is a common practice across the globe as reported in China (Streets et al., 2003; Zhang et al., 2020), South America (Graham et al., 2002), Southeast Asia (Lasko and Vadrevu, 2018; Yin, 2020) and from the northwest India (Singh et al., 2018, 2021; Sarkar et al., 2018). Crop residue burning over northwest India has been investigated widely from diverse perspectives. A widespread intensive burning during October to mid-November is a recurring phenomenon and often associated with poor air quality at downstream (Jethva et al., 2019; Singh et al., 2018), modifying aerosol loading and chemistry (Mhawish et al., 2022; Ravindra et al., 2023), influencing aerosol vertical stratification and radiative forcing (Hsu et al., 2003; Vinjamuri et al., 2020; Banerjee et al., 2021), inducing negative health impacts (Singh et al., 2021), and possibly shifting regional hydrological cycle (Kant et al., 2023).~~ However, limited attention has been paid to investigate its effect on urban climate, especially on modulating lower atmospheric thermal budget which has been otherwise strongly evident in case of forest fire (Liu et al., 2018, 2019).

Across the northwestern ~~part of~~ India, dual cropping pattern including rice and wheat crop is predominately practised over roughly 4.1 million ha of land (NAAS, 2017). Such a cropping pattern leads to ~~results in~~ generation~~ng~~ of huge crop residues ~~having~~ that are low in~~poor~~ nutrient content ~~with~~ and rich in~~high~~ silica and ash ~~fractions~~. Typically, residues from rice-wheat cropping system ~~have~~ possess limited economic value, ~~not being fitted as alternative fodder, biofuel or being procured in pulp and paper industries~~as they are unsuitable for use as alternative fodder, bioenergy feedstock or as raw material in pulp and paper industry (~~Lan et al., 2022;~~ Shyamsundar et al., 2019; Lan et al., 2022). Besides, with the ~~advent~~ introduction of mechanical harvester in the 1980s and enactment of groundwater preservation act in the late 2000s, in situ ~~indiscriminate~~ burning of agricultur~~al~~e residues has

Formatted: Font: 9 pt

~~been~~ become a~~the~~ recurrent ~~choice~~ practice among ~~of~~ the local farmers. This practice serves to expedite field clearance and reduce the turn~~-~~around period~~time~~ between rice harvest~~ing~~ and the subsequent sowing of the wheat crop (Balwinder-Singh et al., 2019).~~ India generates a~~ India produces an estimated 500 million metric tonnes (MT) of crop residues annually, of which 20–25% are disposed of through open-field burning.~~Annually, India produces an estimated 500 million metric tonnes (MT) of crop residues, of which approximately 20–25% are disposed of through open-field burning.pproximately 500 million metric tonnes (MT) of crop residues per year with roughly 20-25% i.e. 100-120 MT/yr residues usually burn in the field itself~~ Crop residue burning is particularly prevalent in northwestern India, where roughly 20-25 MT of residues are set on fire each year ~~, majority (~20-25 MT/yr) of such practised over northwest Gangetic plain~~ (Balwinder-Singh et al., 2019; Lan et al., 2022~~; Balwinder-Singh et al., 2019~~). Unregulated residue burning in this region contributes ~~Unregulated burning of agriculturale residues across the northwestern part of India usually held responsible for~~is ~~estimated to contribute~~ approximately 300 Gg/yr of $PM_{2.5}$ and 50 Tg of CO_2 equivalent green-house gas emission (Singh et al., 2020). ~~Interestingly, fire incidences have exhibited a consistent increasing trend with concurrent growth in vegetation index and aerosol loading~~ Notably, the frequency of fire incidences has exhibited a persistent upward trend, coinciding with concurrent increases in vegetation indices and atmospheric aerosol loading (Vadrevu et al., ~~2018~~2019; Jethva et al., 2019). In addition to atmospheric emissions, fires exert numerous biophysical impacts on the surrounding ecosystems. Fire induces a cascade of consequential processes, including modifications to the surface energy balance, redistribution of nutrients, alterations in species composition, changes in surface albedo, and variations in evapotranspiration rate ~~Beside emissions, biophysical effects of fire on surrounding ecosystem could be many as fire drives several consequential changes, be it in modifying surface energy balance, redistributing nutrients and species, modifying surface albedo thereby, altering evapotranspiration rate~~ (Ward et al., 2012; Liu et al., 2019). Additionally, fire ~~could~~ can ~~also~~ induce certain biogeochemical and biophysical stresses on local environment by modifying atmospheric composition and surface properties (Andela et al., 2017; Aditi et al., 2025). Such transformation ~~in~~of the native landscape, coupled with excessive release of energy, ~~and, emission of~~ aerosols and ~~itstheir~~its precursors, may therefore~~,~~ have several potential implications on the ~~local~~ environment.

Formatted: English (United States)

Formatted: Font: 9 pt

Most studies on biomass-based fires have focused on identifying land–atmosphere processes responsible for fire initiation and propagation, quantifying emissions, and evaluating fire-induced land–atmosphere exchanges (Lasko and Vadrevu, 2018; Jethva et al., 2019; Chuvieco et al., 2021; Aditi et al., 2025). ~~Most studies on biomass-based fires have has focused on identifying the land and atmospheric processes and precursors responsible for fire initiation and propagation, quantifying emissions, and evaluating land–atmosphere exchanges (Lasko and Vadrevu, 2018; Jethva et al., 2019; Chuvieco et al., 2021; Aditi et al., 2025).~~ In contrast, there is a paucity of knowledge regarding how biomass burning contributes to climate feedbacks through modifications of Earth's surface radiative budget and land surface temperature~~.~~ ~~Majority of the researches involving biomass-based fire are dedicated to recognize land and atmospheric processes and precursors on initiating and propagating fire, quantifying emissions and evaluating land surface-atmosphere exchange. There is however, limited understanding on how biomass-based fire induce climate feedback by altering Earth's surface radiative budget and land surface temperature~~ (Bowman et al., 2009; Andela et al., 2017). Plausible explanation to this includes limited observation and associated uncertainties in estimating key biophysical ~~processes~~ parameter like surface albedo, land-atmosphere exchange of sensible heat flux and water vapor, changes in evapotranspiration before and after fire events~~evapotranspiration rate during pre- and post-fire events~~. There are instances when global forest fire incidences and size have been linked with modifications in land surface temperature (LST; Alkama and Cescatti, 2016; Liu et al., 2018, 2019). Likewise, Liu et al. (2019) noted an enhancement in mean annual LST over burned forest area in the northern high latitudes. Similar evidence of increase in summertime surface radiometric temperature over temperate and boreal forests in the Northern Hemisphere was accounted by Zhao et al. (2024). Alkama and Cescatti (2016) reported increases in mean and maximum air temperature over arid regions following forest loss, highlighting the sensitivity of surface temperature to land-cover modification. However, fire-induced thermal forcing is strongly constrained by the fire size (Zhao et al., 2024). Small, short-lived fires, such as those associated with agricultural residue burning, often fail to produce sufficiently large changes in surface albedo or evapotranspiration, and therefore may not generate a detectable LST response. ~~Alkama and Cascatti (2016) evident reported a corresponding increase in mean and maximum air temperature over the arid zone regions due to the loss of forest cover. However, fire-induced thermal forcing was reported to be constrained by fire size (Zhao et al., 2024)~~

Formatted: Font: 9 pt

~~and often, relatively small scale burning, particularly involving crop residues on agricultur~~al~~e farmland may not be sufficient enough to induce robust change in surface albedo and evapotranspiration, resulting insignificant variation in LST.~~ Incidence of elevated LST over different provinces in China due to agricultural~~e~~ residue burning has only recently reported by Zhang *et al*. (2020). A spatially ~~inconsistent~~ heterogeneous increase in LST ~~-~~correlated ~~well~~ strongly with fire count, ~~having~~ with highest LST gradient noted at distances of 4–10 km from the central point of crop residue burning ~~in 4 to 10 km distance from the central point of cop residue burning~~ and ~~remained valid~~persisting ~~till~~ for 1-3 days. In contrast, the effects of post-harvest fire incidences in northwestern India on LST remain largely unexplored. This gap introduces considerable uncertainty in assessing the climate feedback of crop residue burning and highlights the need for a better understanding of the underlying mechanisms~~In contrast, post-harvest fire incidence over northwest India has not yet explored in terms of its effect on LST. This induces significant uncertainty in recognizing climate feedback of crop residue burning and warrants a better understanding of the underlying mechanism~~.

This study aims to explore immediate biophysical effect of agricultural~~e~~ ~~crop~~ residue fire on surface temperature over northwestern India. By integrating spatially and temporally consistent satellite ~~-~~observations and reanalysis datasets, including~~-based observations on~~ fire counts, fire radiative power, land surface temperature, aerosols~~loading~~, meteorological covariates, topography, surface property, and physical environment ~~- and regional meteorology~~ over intensive fire zone, we sought to quantify time-bound changes in LST in ~~relation~~response to variations in fire intensity and aerosol loading~~we tried to establish time-bound changes in LST with concurrent variations in fire strength~~. Several statistical ~~means~~ methods were ~~explored~~ applied to construct the changes in LST with fire severity and aerosols. Additionally, a space-for-time framework was ~~applied~~followed to assess the effects of recurrent FRP variations on LST and aerosol optical depth (AOD) throughout the fire season.~~A space-for-time approach was used to construct changes in LST and AOD due to recurrent changes in FRP over the fire season.~~ Specifically, we addressed two key questions: ~~we tried to investigate two questions,~~ (1) ~~does~~ Does ~~land surface temperature~~LST respond to changes in fire intensity over northwestern India?~~,~~ and (2) ~~how~~ How do local meteorology and aerosol loading modulate LST variation with respect to space and time? To the best of our knowledge, this is the first systematic assessment of agricultural residue fire–driven

Formatted: Font: 9 pt

modulations in LST over northwestern India~~no previous study has systematically analyzed agricultural residue burning driven changes in LST over northwestern India~~. By integrating multiple geospatial observations, the analysis offers critical insights into the biophysical feedbacks of residue-based fire and advances understanding of LST responses to residue burning. Further, it refines estimates of fire-induced perturbations in the regional radiative budget offering valuable representation of biomass-based fire in Earth system models.

Formatted: Font: Font color: Text 1, Ligatures: Standard + Contextual

~~Such an investigation could provide critical insights into the biophysical feedbacks of fire on surface temperature and radiative budget from crop residue burning.To best of our knowledge, such understanding on regulated in LST explorednortherncouldvital evidence onfeedback from based fire~~.

2. Dataset and methodology

2.1 Study domain

~~Post-harvest burning of biomass is mainly practised over the northwest part of the Indo-Gangetic Plain (IGP) of South Asia. The region encompassing the agrarian states of Punjab and Haryana is particularly productive and accounts for a whopping 60-70% of India's food grain generationproduction. Coupled with increased production of rice and wheat crop, generation of crop residues has been increased multi-fold in recent years resulting higher intensity in crop-based fire over the region (Jethva et al., 2019). For this research, the geospatial analysis of LST in continuation with fire activity and aerosol loading has been made over the northwest part of India for the months of October to November between year 2017 and 2021. The combination of high agricultural output, extensive biomass burning, and documented increases in fire activity renders this region specifically appropriate for analysing fire dynamics and their environmental consequences. However, instead of pre-identifying a fixed research domain, we have retrieved year-wise fire signal across the northwest India constrained by crop land. This led to the selection of core-study region differs annually with respect to year-specific fire intensity and spatial trend (as in Fig. S1, in supplementary file), but all eventually bound to 29.2770° to 32.1625° N and 73.8996° to 77.0718° E, as illustrated in Fig. 1b.~~

Formatted: Font: 9 pt

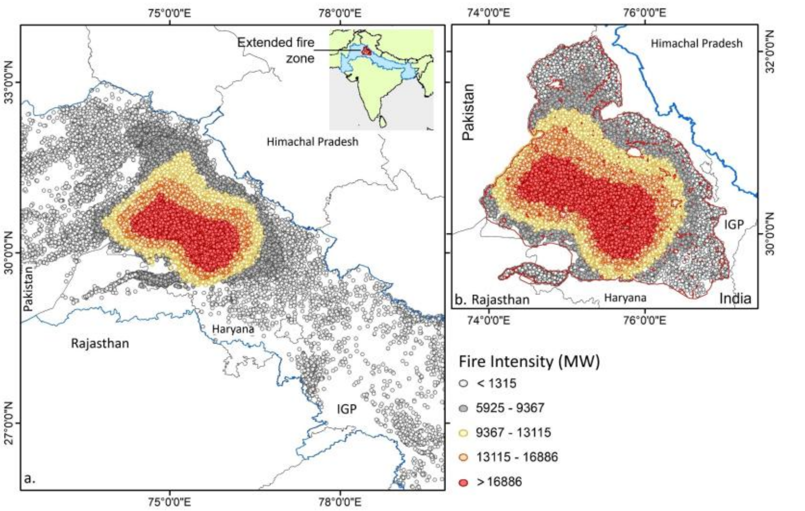

Fig. 1. Spatial variation in satellite-based fire radiative power across northwest India, distribution of FRP-based fire intensity (MW/pixel) (a) and domain selected for retrieval and processing of SNPP VIIRS FRP, AOD and Aqua MODIS LST (b).

~~NOTE.~~ The region marked with blue in Fig. 1a subset indicates the Indo-Gangetic Plain (IGP) spanning from Pakistan to Bangladesh through India. The extended fire zone selected for analysis is marked with red within the IGP and has been shown in detail in Fig. 1a with fire pixel density. ~~The selection criteria of the spatial domain are discussed in section 2.3. The pixel size of VIIRS VNP14IMG is 375x375 m^2.~~ India shape file is acquired from Survey of India archive.

Post-harvest biomass burning is predominantly practiced across the northwestern Indo-Gangetic Plain (IGP) of South Asia, particularly in the agrarian states of Punjab and Haryana, which together contribute nearly 60–70% of India's total food grain production. The concurrent rise in rice and wheat cultivation has led to a substantial increase in crop residue generation, resulting in higher fire intensity in recent years (Jethva et al., 2019). In this study, geospatial analyses of LST, fire activity, and aerosol loading were conducted over northwestern India during October–November between 2017 and 2021. The combination of high agricultural output, extensive biomass burning, and increasing fire activity makes this region particularly suitable for investigating fire dynamics and their environmental

Formatted: Left, Indent: First line: 0 cm

Formatted: Font: 12 pt

Formatted: Line spacing: 1.5 lines

Formatted: Indent: First line: 1.27 cm

Formatted: Font: 9 pt

implications. Instead of defining a fixed spatial domain a priori, year-wise fire signals were retrieved across cropland areas in northwestern India. This approach allowed the delineation of a core study region that varied annually according to year-specific fire intensity and spatial trends (as shown in Fig. S2), but all eventually bound to 29.2770° to 32.1625° N and 73.8996° to 77.0718° E, as illustrated in Fig. 1b.

Formatted: Font: Not Bold

2.2 Spatial dataset

Active fire count data was retrieved from the standard fire product of Visible Infrared Imaging Radiometer Suite (VIIRS) Collection-2 ~~Level 1B~~ (VNP14IMG) available at 6-min L2 swath at 375 m resolution. The VIIRS onboard the Suomi National Polar-orbiting Partnership (SNPP) satellite is a cross-track single-angle scanning radiometer which was launched in year 2011 under joint operation of NASA and NOAA. The VIIRS fire detection algorithm typically extends well refined and validated MODIS Fire and Thermal Anomalies product (Giglio et al., 2003). The I-band based fire detection algorithm primarily utilizes brightness temperature of Channel I4 on middle infrared spanning from 3.55 to 3.93 µm, centred at 3.74 µm. Additionally, to isolate the active fire spots from the fire-free background channel, a single gain I5 at thermal infrared regions (10.5–12.4 µm) is also considered. Rest of the I-band channels i.e. I1 to I3, covering visible, near and short-wave IR are used to distinguish pixels with cloud, water and sun-glint (Schroeder et al., 2014). The VIIRS fire database was considered due to its superior precision and accuracy in identifying relatively small fire, greater spatial resolution at footprint and pixel saturation temperature (Li et al., 2018; Vadrevu ~~et al.,~~and Lasko, 2018; ~~Li et al., 2018;~~ Aditi et al., 2023). For this experiment, SNPP VIIRS 375 m ~~C2~~ L2~~1B~~ active fire count data with nominal (fire mask class 8) and high confidence (fire mask class 9), was retrieved over northwestern India from year 2017 to 2021 (all inclusive).

Fire radiative power (FRP) quantifies the release of radiative energy from biomass burning integrated at all angles and wavelengths over a spatial scale. Measured in Watt, FRP retrieval quantifies the release of heat energy against time and in many instances linearly associated with the rate of fuel consumption and emission (Ichoku et al., 2008; Nguyen and Wooster, 2020). A detailed description on FRP retrieval and comparison among the sensors are available in Wooster et al. (2003, 2005) and Ichoku et al. (2008). Li et al. (2018) concluded VIIRS FRP as comparable with MODIS FRP in most of fire clusters and ~~very~~ stable across swath.

Formatted: Font: 9 pt

Here, FRP (MW) was processed from the SNPP VIIRS C2 Level-2 (L2) 375 m active fire product (VNP14IMG). VIIRS FRP was used as a proxy of fire intensity and potential emission strength from the biomass burning area, and considered as a direct measurement of radiative energy being released from individual fire pixel.

Land surface ~~radiometric~~ temperature (LST, in °C) at 1 km spatial resolution was utilized from Moderate Resolution Imaging Spectroradiometer (MODIS) version 6.1 Land Surface Temperature and Emissivity retrievals product (MYD11A1). Typically, LST indicates thermodynamic temperature of the interface atmospheric layer within soil, plant cover and lower atmosphere, and serves as an indicator of land-atmosphere interaction and exchange (Li et al., 2023). Here, MODIS MYD11A1 radiometric dataset with quality flag '00' was specifically chosen considering its broad swath and wider applicability in estimating land surface temperature. ~~Besides,~~ MODIS LST is validated against ground observations on diverse land covers and reported to provide realistic estimate of surface temperature (Wan, 2014) with an uncertainty of ≤0.5 K. The dataset includes daytime maximum LST (at 1:30 PM local time) and nighttime minimum LST (at 1:30 AM local time). ~~Both daytime maximum and nighttime minimum LST approximately at 1:30 PM and 1:30 AM local time respectively, are available.~~ ~~However~~Here, daytime LST dataset were obtained solely from the MODIS sensor onboard the Aqua satellite to closely coincide with VIIRS fire count observations at 1:30 PM local time, a period when crop residue–based fires are expected to reach at peak~~, to better approximate the timing of VIIRS fire count retrieval at 1:30 PM local time when crop residue-based fire presumably remains at peak, surface retrievals of LST was only made from MODIS onboard Aqua satellite~~.

Aerosol optical depth (AOD) from Visible Infrared Imaging Radiometer Suite (VIIRS) sensor on-board SNPP satellite offers accurate estimation of columnar aerosol loading at 550 nm over land. Accuracy of VIIRS V1 DB AOD was evaluated extensively over South Asia by Aditi et al. (2023) and reported to provide stable AOD retrieval against AERONET. Sayer et al. (2019) reported an estimated error of ±(0.05+20%) in VIIRS Version 1 DB AOD dataset. Here, Deep Blue (DB) Version 1 AOD dataset (AERDB_L2_VIIRS_SNPP Level-2) was used to retrieve AOD with a nominal spatial resolution of 6 km at nadir. Only quality assured AOD (QA ≥ 2) was

Formatted: Font: Not Italic

Formatted: Font: Not Italic

Formatted: Font: 9 pt

retrieved for the months of October to November ~~for years 2017 to 2021~~ over selected spatial domain.

Terra/Aqua MODIS land cover data was used to discriminate crop land against the rest to filter out thermal anomalies exclusively over the agriculture land. To achieve this, MODIS L3 V6.1 Global Land Cover type product (MCD12Q1) was retrieved from LAADS DAAC site for year 2017, available at 0.5 km spatial resolution. MODIS land cover types adopts International Geosphere-Biosphere Programme (IGBP) and other land type classification schemes to classify land cover. Here, land cover type 12 (cropland) was earmarked to isolate the agriculture land from its surrounding (Fig. S3~~2~~).

Daily composite data on surface and root-zone soil moisture (SM, m^3 m^{-3}) available at 9 km resolution was obtained from NASA's Soil Moisture Active Passive (SMAP) satellite mission having L-band radar. The Normalized Difference Vegetation Index (NDVI) at 6 km resolution was derived from the VIIRS/SNPP Deep Blue (AERDB_L2_TOA_NDVI) dataset and was utilized to quantify surface vegetation greenness dynamics. Elevation data at 30 m resolution was retrieved from Copernicus DEM - Global and European Digital Elevation Model dataset for year 2015. Surface albedo data was acquired from MCD43 suite of NASA standard product which integrates both Terra and Aqua retrievals. Here, white-sky version 6.1 shortwave albedo data (MCD43A3, Albedo_WSA_shortwave) at 500 m pixel resolution with daily-time step (quality score: 0) was used.

Lower surface meteorological data including air temperature (~~At~~AT), total solar radiation flux (~~Sr~~SR), precipitation (P~~r~~R), ~~and~~ relative humidity (RH) was procured from European Centre for Medium-Range Weather Forecasts (ECMWF) AgERA5 dataset. The AgERA5 dataset has been generated by Copernicus Climate Change Service (2020) from hourly ECMWF ERA5 dataset for specific agro-ecological based applications. The meteorological data were pre-customized with temporal aggregation aligned to local time zones and spatial enhancement to a 0.1° resolution using grid-based variable-specific regression model. Here, air temperature at 2 meters above the surface, total solar radiation flux received at the surface over a 24-hour time period, and relative humidity at 2 m~~eter~~ height was selectively used over pre-identified intensive crop-based fire zone. Planetary boundary layer height (PBLH) data at 0.25° x 0.25° resolution was acquired from ECMWF ERA5 for 13:00-14:00 h local time

Formatted: Font: 9 pt

corresponding with VIIRS overpass time. A description of all core datasets used in this analysis and their resolution, version, and quality flags ~~and level of uncertainty~~ is included in Table S1 (in supplementary file).

2.3 Spatial analysis for fire-aerosols-LST association

2.3.1 Selection of intensive fire zone

Post-harvest residue burning typically begins in mid-October and reaches peak intensity by mid-November across northwestern India. Accordingly, all spatial analyses were conducted for October and November for the years 2017–2021. The VIIRS 375 m fire product successfully retrieved active fire pixels across the Indo-Gangetic Plain, capturing substantial spatial heterogeneity. ~~Post-harvest specific crop residue burning typically commences during mid-October and reaches its peak intensity during mid-November, particularly over northwest India. All the spatial analysis was therefore, conducted for the months of October and November for year 2017 to 2021 (all inclusive). The VIIRS 375 m fire product was able to retrieve active fire pixels across the IGP with marked spatial heterogeneity.~~ To ascertain a representative region having predominance of residue-based fire, spatial comparison of fire pixel density was made using daily retrieved VIIRS FRP dataset. FRP was selected instead of fire counts because it directly quantifies the radiative energy released from active burning and therefore provides a more meaningful metric for assessing potential impact~~s~~ on LST. FRP density was computed on a 1.5 × 1.5 km^2 grid to characterize spatial variations in fire intensity across northwestern India. Following Giglio et al. (2006), FRP density was estimated as the ratio of total FRP within a grid cell to the grid area.~~The selection of FRP over fire count as a criterion to isolate intensive fire region was driven by the fact that FRP directly relates energy release from active fire thereby, potentially modulate the spatial change in LST. Pixel density of fire radiative power was assessed at 1.5 x 1.5 km grid to compare spatial variations in FRP intensity across northwest India. To compute FRP density, a ratio between FRP and the grid area was computed following the protocol mentioned in Giglio et al. (2006).~~

~~Initially, geospatial variations in fire intensity and associated changes in LST and AOD was assessed. Spatial intercomparison between fire intensity with LST and AOD was made over the designated zone shown in Fig. 2a. The zone was earmarked to cover an extended geographical area without imposing any discrimination between low and high FRP density over the northwest India. The zone was henceforth, referred as '*extended geographical*~~

Formatted: Font: 1 pt

Formatted: Superscript

Formatted: Font: 9 pt

~~*region'* as it combines fire intensity across the years and was solely meant to constitute spatial association between the dependent and predictor variables.~~

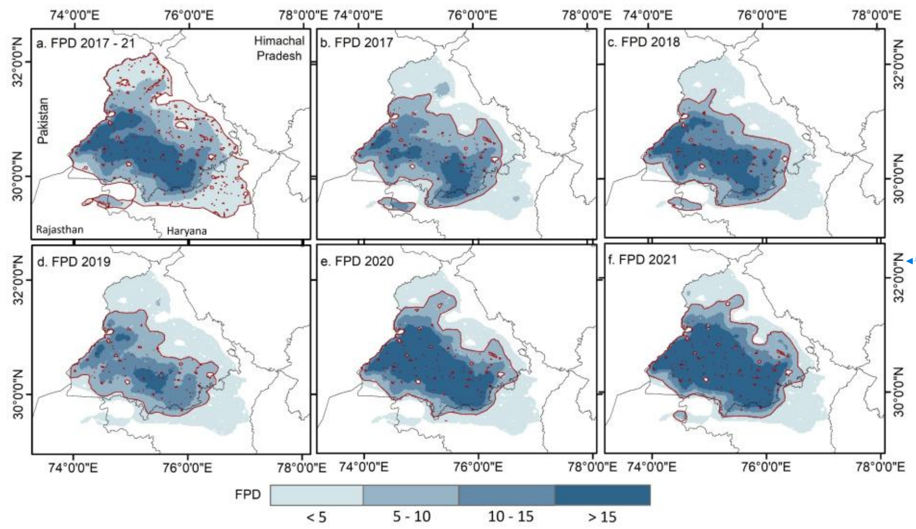

Fig. 2. Selection of high intensity residue-based fire zone based on fire radiative power pixel density (MW 2.25 k~~K~~m^{-2} day^{-1}).

~~NOTE.~~ Fig. 2a indicates the '*extended geographical region*' demarcating the entire area with varying fire intensity selected for spatial analysis. Rest of the figures classify year-specific '*intensive fire zone*' ~~used to retrieve all the variables for spatiotemporal analysis~~ based on FRP density.

Initially, geospatial variations in fire intensity and the associated changes in LST and AOD were evaluated. Spatial intercomparison between FRP, LST, and AOD was performed over the region delineated in Fig. 2a. This area was selected to encompass an extended geographical domain without imposing thresholds on low or high FRP density across northwestern India. The region is hereafter referred to as the "extended geographical region," as it integrates fire activity across all years and was used exclusively to establish the spatial association between the predictor (FRP) and dependent variables (LST and AOD).

In contrast, to assess the day-to-day influence of fire intensity and aerosol loading on LST, a comparatively high-intensity fire zone was delineated relative to low-intensity areas. To achieve this, the entire crop-residue burning region of northwestern India was mapped using a constraint from low FRP density (<5 MW grid^{-1}) to high FRP density (>15 MW grid^{-1}).

Formatted: Justified

Formatted: Font: 12 pt

Formatted: Space Before: 3 pt

Formatted: Font: 12 pt, Italic

Formatted: Font: Italic

Formatted: Font: 12 pt, Italic

Formatted: Font: 12 pt

Formatted: Font: 12 pt, Italic

Formatted: Font: 12 pt

Formatted: Font: 12 pt

Formatted: Font: 9 pt

Spatial variations in FRP density were evaluated for each year, and regions with FRP density >5 MW grid^{-1} were identified as the “intensive fire zone” (Fig. 2b–f). ~~In contrast, to establish potential effect of day to day variations in fire intensity and aerosol loading on LST, comparatively high intensity fire zone was designated against low intensity zone. To achieve this, entire crop-residue burning region of northwest India was earmarked constraining low (<5 MW grid^{-1}) to high FRP density (>15 MW grid^{-1}). Spatial variations in FRP density were compared among the selected years and region(s) was identified considering a threshold FRP density >5 MW grid^{-1} area (Fig. 2b-f).~~ This threshold ensured a better representation of the effect of medium to large crop-based fire on regional LST as ~~very~~ small-intensity fire deem to extinguish faster while being inconducive to considerably influence surface temperature (Zhao et al., 2024).

All subsequent spatial datasets used for evaluating FRP–AOD–LST relationships were retrieved exclusively within the year-specific ‘intensive fire zone’ having FRP density >5 MW grid^{-1}. Notably, the spatial extent of the high-FRP region remained largely consistent across all years (Fig. 2b–f), with areal estimates summarized in Table S2. ~~All the spatial datasets were subsequently retrieved exclusively within the year-wise designated ‘*intensive fire zone*’ having FRP density >5 MW grid^{-1}, and included for ascertaining FRP-AOD-LST association. Incidentally, area having high FRP density (>5 MW grid^{-1}) remained almost consistent as illustrated in Fig. 2(b-f) and quantified in Table S1.~~ It is noteworthy, the ~~fire intensive~~ region was pre-filtered based on the Terra/Aqua MODIS land cover data to deselect any FRP pixel that emerged from a non-agricultural/crop land.

2.3.2 Selection of temporal window

After isolating the region with higher fire pixel density, the next step was to identify the temporal window in which potential associations between fire intensity and other explanatory variables could be examined. The temporal selection was based on two scenarios, as illustrated in Fig. 3. Scenario 1 was designed to quantify the influence of FRP, aerosols, and other parameters on LST during the period when fire activity begins to intensify and remains persistent over the intensive fire zone. Scenario 1 defines the initiation day as the first instance in October when aggregate FRP consistently exceeds 1500 MW and shows at least a 50% increase compared to the previous day. The scenario concludes in November when aggregate FRP decreases by at least 50% relative to the previous day. The selected dates for Scenario 1

Formatted: Font: (Default) Calibri, Font color: Text 1, Ligatures: Standard + Contextual

Formatted: Font: (Default) Calibri, Font color: Text 1, Ligatures: Standard + Contextual

Formatted: Font: 9 pt

are listed in Table S3, with two exceptions. ~~As the region with higher fire pixel density was isolated, our subsequent effort was to identify temporal window to assess potential association between fire intensity and other explanatory variables on the identified zone. Selection of temporal window for spatial analysis was based on two scenarios as illustrated in Fig. 3. Scenario (1) was to quantify the influence of FRP, aerosols and other parameters on LST when fire intensity starts to build up and remain persistent over the intensive fire zone. Scenario (1) therefore, considers the day as initiation when FRP starts to build up for the first time in October and consistently exceeds 1500 MW with a corresponding 50% increase in area weighted FRP aggregate against its previous day. The Scenario (1) concludes with the same approximation during November with a 50% decline in aggregate FRP compared to its previous day. The dates selected for scenario (1) are shown in Table S2 with two exceptions.~~ First, in year 2018 when a >50% criteria was not met despite having an aggregate FRP >1500 MW and second, in year 2017 when a prior decrease (>50%) in FRP was avoided because of subsequent rise in fire intensity.

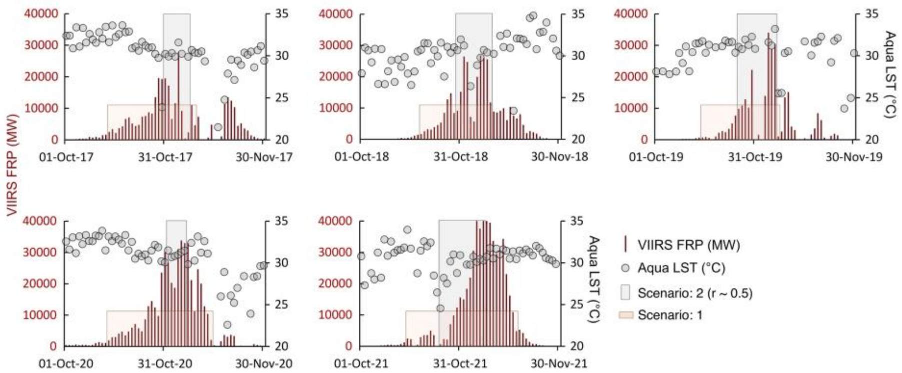

Fig. 3. FRP and LST time series ~~against LST~~ over ~~year-specific~~ intensive fire zone showing the extent of ~~with marked time frame for both~~ scenarios ~~selected~~ used for geospatial modelling.

~~NOTE. All the spatial datasets including FRP, fire count, AOD and LST were retrieved exclusively within the year-wise designated fire intensive zone having FRP density >5 MW grid^{-1}. Scenario (1) refers extended timeframe to consider entire fire period while scenario (2) select the interlude having high temporal coefficient between FRP and LST.~~

Formatted: Font: 12 pt

Formatted: Indent: Left: 0 cm, Hanging: 1.25 cm, Line spacing: 1.5 lines

Formatted: Font: 9 pt

To define Scenario 2, a statistical association was examined between day-specific aggregate FRP and the spatially averaged LST. Pixel-based LST values were averaged over the intensive fire zone and compared against the area-weighted sum of FRP on a day-to-day basis. A temporal window ("Scenario 2" in Fig. 3) was selected using two criteria: (i) the end of the window had to coincide with a period of persistently high FRP, and (ii) the window had to exhibit a strong positive correlation ($r \geq 0.5$) between FRP and regional LST. ~~To constitute scenario (2), statistical association between day-specific aggregate FRP and spatially average LST retrievals were examined. Precisely, pixel-based LST was averaged over intensive fire zone and compared against area weighted FRP sum on day-to-day basis. Here, a temporal window ('*Scenario: 2*' in Fig. 3) for spatial analysis was identified to fulfilling two criteria; first, the end date of the window should coincide with the day having relatively high FRP and second, the selected window should achieve a robust and positive correlation (r ≥0.5) between FRP and LST.~~ Such restricted criteria were put to ensure that we only select year-specific window(s) when FRP (so the fire count) increases with time and exhibit a strong association with regional LST. Descriptive statistics of both scenarios are included in Table S4. It is noteworthy that selecting multiple windows within a year having coinciding days was avoided while ensuring windows should not contain more than 5% of missing days, irrespective of parameters.

2.4 Spatial correlation between fire, aerosols and LST

To examine the spatial association among FRP, LST, and AOD over the residue–based fire zone, grid-based spatial correlation coefficients were computed, and their statistical significance ($p < 0.05$) was tested across the study domain. Daily FRP (375 m) and LST (1 km) datasets were initially resampled to a 6x6 km^2 resolution to match the VIIRS AOD dataset before subject to spatial correlation analyses among the predictor and dependent variables. This approach facilitated the identification of regions exhibiting strong co-variability in thermal conditions corresponding to variations in fire intensity and columnar aerosol loading.~~To identify spatial association between FRP, LST and AOD over the crop residue-based fire zone, pixel-based spatial correlation coefficient was computed and its statistical significance (P<0.05) was tested across the study domain. This enables us to identify region having robust co-variability across the thermal conditions with varying fire intensity and columnar aerosol loading.~~

Formatted: Indent: Left: 0 cm, Hanging: 1.25 cm

Formatted: English (India)

Formatted: Line spacing: 1.5 lines

Formatted: Superscript

Formatted: Font: 9 pt

2.5 Hurst Exponent

The Hurst exponent is a statistical measure used to characterize the properties of a time series without imposing assumptions about its underlying distribution. Originally introduced by Hurst (1951) in hydrological studies and later refined by Markonis and Koutsoyiannis (2016), it has since been widely applied across diverse scientific disciplines to analyse long-term trends and variability. In this study, the Hurst exponent was computed for FRP, AOD, and LST time series to identify long-term statistical persistence in the datasets. To estimate the Hurst exponent at the spatial scale, 6 × 6 km² resampled datasets of FRP, AOD, and LST were used. Adjustment of seasonal cycle was not accounted, as the datasets were retrieved and processed exclusively for a single season across the selected years. ~~The Hurst exponent is a statistical measure used to characterize the properties of a time series without imposing assumptions regarding its statistical distribution. Originally introduced by H.E. Hurst (1951) in the context of hydrological studies and later refined by Markonis and Koutsoyiannis (2016), it has since been widely applied across diverse scientific disciplines for analysing long-term trends and variability. Here, Hurst exponent was computed for FRP, AOD and LST timeseries to recognize long term persistence of the dataset.~~ The main calculation procedures were as follows (Granero et al., 2008):

A time series x(t) is given,

$$(\mathrm{x})_{\mathrm{t}} = 1/\tau \sum_{t=1}^{\tau} x(t) \quad t = 1, 2, 3 \ldots \qquad (1)$$

The cumulative deviation is determined using Eq. 2:

$$X(t,\tau) = \sum_{u=1}^{\tau}(x(u) - (\mathrm{x})_{\mathrm{t}}), \text{ with a condition of } 1 \le t \le \tau. \qquad (2)$$

Extreme deviation sequence, is defined as:

$$\mathrm{R}(\tau) = \max_{1\le t\le\tau} \mathrm{X}(t,\tau) - \min_{1\le t\le\tau} \mathrm{X}(t,\tau) \quad where\ \tau = 1, 2, 3 \ldots \qquad (3)$$

The standard deviation sequence is calculated by Eq. (4):

$$S(\tau) = [1/\tau \sum_{t=1}^{\tau}(\mathrm{x(t)} - (X)_{\tau})^2]^{1/2} \quad where\ \tau = 1, 2, 3 \ldots \qquad (4)$$

By considering both extreme deviation sequence and standard deviation sequence,

$$R/S = R(\tau)/S(\tau) \text{ when assuming } (R/S) \propto (\tau/2)^{H} \qquad (5)$$

Formatted: English (United States)

Formatted: Line spacing: 1.5 lines

Formatted: Font: 9 pt

The Hurst exponent ranges between 0 and 1. A value of 0.5 indicates that the time series behaves as a purely stochastic process without persistence, implying that future variations are independent of past behaviour. Values greater than 0.5 denote statistical persistence, reflecting a tendency for future changes to follow the same trend as in the past, with higher values corresponding to stronger persistence. Conversely, values below 0.5 indicate anti-persistence, suggesting a tendency for the time series to reverse its trend over time; lower values represent stronger anti-persistence (Peng et al., 2011).~~Hurst exponent varies between 0 and 1. A value of 0.5 signifies that the time series behaves as a stochastic process lacking persistence, indicating that future trends in the series are independent of those observed during the study period. Values exceeding 0.5 denote persistence in the time series, reflecting a tendency for future changes to follow the same trend as in the past; higher values correspond to stronger persistence. Values below 0.5 indicate anti-persistence, meaning the time series exhibits a tendency to reverse its trend over time, with lower values indicating stronger anti-persistence (Peng et al., 2011). To compute Hurst exponent at spatial scale, 6x6 km² resampled datasets of FRP, AOD and LST were used.~~

2.6 Space-for-time approach

A space-for-time approach was employed to assess and compare the ~~spatial heterogeneity~~changes in~~of~~ LST and AOD with respect to ~~variations in~~ FRP within the extended geographical region experiencing recurrent medium- to ~~large~~high--intensity fire. To ~~ascertain that the~~ensure that changes in LST and AOD were attributable solely to fire activity, grids with similar characteristics in terms of topography, climate, and physical environment were compared (Liu et al., 2019)~~was only due to fire, we have adopted the procedure briefed in Liu et al. (2019) where grids exhibiting fire were only compared with control grids having similar characteristics~~. To achieve this, daily datasets including meteorological covariates (PBLH, AT, SR, RH and PR), physical environment (elevation), vegetation and soil characteristics (NDVI, soil moisture), climatological mean LST and AOD, and surface property (albedo) were extracted over both fire and no-fire grids at a spatial resolution of 10 × 10 km²~~climatological mean LST and AOD, and systematic land-cover differences (albedo) across the fire and no-fire grids were extracted in multiples of 10x10 km² grid cell and compared~~. The daily data were retrieved for each grid ~~during~~under Scenario 2, when FRP reached its peak and exhibited a

Formatted: Font: 9 pt

positive association with regional LST.~~Daily LST, AOD and FRP~~~~dataset was subsequently retrieved over individual grid for the duration selected under scenario two when~~ ~~FRP remains at its peak and corresponds a~~ ~~both fire and corresponding LST increases with time~~~~positive association with regional LST.~~

~~A space-for-time approach (Liu et al., 2019) was used to assess and compare heterogeneity in AOD and LST against the variation in FRP within residue based fire zone. Initially, year specific intensive fire zone was categorically divided in to multiples of 10x10 km^2 grid cell, selected on the basis of resolution of VIIRS AOD.~~ ~~Daily LST, AOD and FRP was subsequently retrieved over individual grid for the duration selected under scenario two when both fire and corresponding LST increases with time.~~ After filtering out the grid cells ~~having~~ with missing ~~values for either~~ LST or AOD values, remaining grids were classified into two groups:~~,~~ those with ~~one, having~~ zero FRP (no-fire) against ~~all~~ the grids having FRP > 0, indicating presence of fire. Fire and no-fire grids with comparable spatial characteristics were grouped into a single stratum, and a stratified matching technique was applied to generate multiple strata based on combinations of the selected confounders. Grids were retained only when differences in their physical environment, vegetation and~~,~~ soil characteristics, climate and land cover between fire and no-fire conditions were smaller than the defined thresholds (Δelevation < 50 m; ΔNDVI <0.05; Δsoil moisture <0.05; Δalbedo <0.05; ΔLST <10.0; ΔAOD <0.80). ~~Fire and no-fire grids exhibiting comparable spatial characteristics were grouped into a single stratum, and a simple stratified matching technique was applied to generate multiple strata based on combinations of the selected confounders.~~ Comparisons were then made within strata containing grids of similar attributes to ensure that the observed variations in LST and AOD could be attributed solely to fire activity~~Comparisons were subsequently made within strata containing grids of similar characteristics to ensure that observed changes in LST and AOD could be attributed solely to fire activity~~. The difference in LST (ΔLST) among the fire grids (LST_{fire}) and grids exhibiting no-fire ($LST_{no-fire}$) having similar attributes were compared to constitute effect of residue-based fire on LST. ~~thewithin a strata based fire and having similar attributes~~A positive (negative) ΔLST ($LST_{fire} - LST_{no-fire}$) indicates fire-induced warming (cooling) and was used to quantify changes in LST associated with residue burning for the

Formatted: Indent: First line: 1.27 cm

Formatted: Font color: Text 1

Formatted: Font color: Text 1

Formatted: Not Highlight

Formatted: Font color: Text 1

Formatted: Font: 9 pt

selected years. A similar approach was also adopted to evaluate ∆AOD variations using grid-based retrievals.

It is noteworthy that the grids were not classified based on meteorological covariates, as only insignificant variations were noted among the grids. The entire northwestern cropland experiences a relatively uniform background climate during October–November, including comparable boundary layer heights, with PBLH standard deviations ranging from ±10 m to ±33 m within a single fire season. The climatological mean LST and AOD were computed only for the pre-fire season (September, 2017-2021), during which none of the grids experienced residue-burning activity. Furthermore, grids were not differentiated by slope or aspect, given the minimal topographic variation across the Gangetic Plain.~~It is noteworthy that all grids exhibited a similar background climate, including comparable boundary layer heights with PBLH standard deviation varied from ±10 m to ±33 m within fire season. The climatological mean LST and AOD was included only for pre-fire season. Additionally, grids were not differentiated by slope or aspect, as topographic variation across the Gangetic Plain is minimal.~~

Formatted: Indent: First line: 1.27 cm

~~Subsequently, LST and AOD across all the grids with zero FRP were averaged ($LST_{no\ fire}$) and compared against mean LST (LST_{fire}) computed by averaging the grids exhibiting residue-based fire. A positive (negative) ∆LST (LST_{fire} – $LST_{no\ fire}$) indicates a warming (cooling) induced by fire and was used to assess change in LST due to residue-based fire for the selected years. A similar approach was also used to constitute AOD variations utilizing grid-based retrievals.~~

2.7 Multicollinearity assessment

~~Multicollinearity, where independent variables are highly correlated, can distort regression model estimates and obscure the true relationships between predictors and the target variable (Graham, 2003). In this study, multicollinearity was assessed by calculating the Variance Inflation Factor (VIF) using the statsmodels library. A VIF value of 1 indicates no multicollinearity, values between 1 and 5 suggest moderate correlation, and values above 5 indicate significant multicollinearity (Daoud, 2017).~~ +SR

Formatted: Font: 9 pt

Multicollinearity, where independent variables are highly correlated, can distort regression estimates and obscure the true contribution of individual predictors (Graham, 2003). To assess this, the Variance Inflation Factor (VIF) for all covariates was calculated using the *statsmodels* library. A VIF of 1 indicates no correlation, values between 1 and 5 suggest moderate correlation, and values greater than 5 are generally interpreted as evidence of substantial multicollinearity (Daoud, 2017). All biophysical, land-surface, and meteorological variables met acceptable VIF thresholds, except solar radiation, which was therefore excluded from Random Forest and GWR analysis. Additionally, soil moisture data was removed from ~~ensemble modelling and GWR~~further analysis due to a high percentage of missing observations (~30%).

2.8 Random Forest regression ~~(CHECK REFERENCE) + SM~~

Random Forest regression was used to model the relationship between the dependent variable (LST) and predictor variables (AOD, PBLH, AT, RH, SR, PR, NDVI, elevation, albedo, and FRP) within the intensive fire zone. Daily retrievals, averaged over the year-specific intensive fire area, were incorporated into the ensemble framework to capture potential non-linear associations among variables. The selected approach ensures robustness to multicollinearity, minimizes overfitting, and effectively captures complex predictor interactions.

Random Forest is a non-linear ensemble machine learning algorithm that constructs multiple decision trees from bootstrapped samples of the training data, with a random subset of predictors evaluated at each split. Final predictions are obtained by averaging all trees, improving generalization and reducing overfitting (Breiman, 2001; Puissant et al., 2014). The algorithm was selected due to its strong predictive capability, scalability to large environmental datasets, resilience to correlated inputs, and demonstrated success in previous LST-related studies (Logan et al., 2020; Wang et al., 2022; Zhang et al., 2025). These attributes collectively support Random Forest as an appropriate and interpretable choice for assessing the complex interactions between fire intensity, aerosol loading, and LST dynamics.

~~Random Forest regression was used to model the relationship between the dependent variable (LST) and the predictor variables (AOD, PBLH, AT, RH, SR, PT, NDVI, Elevation, albedo, and FRP). The Random Forest model was applied to daily spatial averages of each dataset to quantify day-to-day changes in surface temperature. Random Forest is a~~

Formatted: Not Strikethrough

Formatted: Indent: First line: 1.27 cm

Formatted: Font: 9 pt

~~non-linear ensemble learning method that constructs multiple decision trees using bootstrapped samples of the training data, with a random subset of predictors considered at each node split. The final prediction is obtained by averaging the outputs of all trees, which enhances generalization performance and reduces overfitting (Breiman, 2001; Puissant et al., 2014).~~

~~Random Forest (RF) regression was used to model the relationship between the dependent (LST) and the predictor variables (AOD, At, RH, Sr, Pr, FRP). It is noteworthy that RF was employed on daily-based spatial average of individual dataset to model the change. The RF is a non-linear ensemble learning method that constructs multiple decision trees using bootstrapped samples of the training data, with random subsets of predictors considered at each split. The final prediction is obtained by averaging the outputs of all trees, which improves generalization and mitigates overfitting. Due to its ability to model complex non-linear relationships and handle multicollinearity and interactions among predictors effectively, RF is particularly suited for environmental modelling tasks (Breiman, 2001; Puissant et al., 2014).~~

Key Rando~~n~~m Forest hyperparameters (n_estimators, max_depth, min_samples_split, min_samples_leaf, and max_features) were optimized using Bayesian optimization implemented via BayesSearchCV in *scikit-optimize* (Snoek et al., 2012; Shahriari et al., 2015; Frazier, 2018). This adaptive, probabilistic search strategy efficiently identifies near-optimal hyperparameter combinations while minimizing computational cost. To ensure robust model evaluation and mitigate temporal dependence, we employed temporal block cross-validation using a 3-fold GroupKFold in the *scikit-learn* library, where all observations from a given year were assigned to the same fold. This approach prevented temporal overlap between training and validation datasets and reduced information leakage across years. ~~The predictive skill of the Random Forest model was evaluated using temporal block cross-validation implemented with GroupKFold, where each fold corresponded to a distinct year.~~ This approach also minimized temporal autocorrelation and prevented data leakage across time periods. Model performance was quantified using cross-validated coefficient of determination (R^2), Root Mean Squared Error (RMSE), and Mean Absolute Error (MAE), providing a comprehensive assessment of model accuracy and prediction error.~~The RF model was implemented using Scikit-learn's RandomForestRegressor with 100 trees and a fixed~~

Formatted: Font: 9 pt

~~random seed to ensure reproducibility. A correlation pattern of prime predictor with dependent variable was also plotted through partial dependence plots (PDPs). The dataset was partitioned into training (75%) and testing (25%) subsets, and model performance was assessed using statistical metrics like coefficient of determination (R^2), Root Mean Squared Error (RMSE), and Mean Absolute Error (MAE), allowing a comprehensive evaluation of model accuracy and prediction error.~~

2.9 Assessment of relative feature importance

Variable importance was derived from the trained RF model using the mean decrease in impurity method, which quantifies each predictor's relative contribution to reducing variance in model predictions. This approach provides insight into the dominant factors governing the spatial and temporal variability of LST. Feature importance values were extracted and ranked to identify the most influential predictors under different fire intensity scenarios. To enable direct comparison among predictors, the relative contribution of each feature was expressed as its importance score normalized by the sum of all feature importances. As Scikit-learn's RandomForestRegressor.feature_importances_ inherently returns normalized values summing to one, the reported scores directly represent each predictor's proportional influence within the model.~~Variable importance was computed from the trained RF model using the mean decrease in impurity approach, which quantifies the relative contribution of each predictor variable in reducing variance in the model's prediction. This analysis offers a focused understanding of the dominant variables driving spatial and temporal variability in LST. Feature importance were extracted and ranked to identify the most influential predictors of LST during diverse fire intensity scenarios. To facilitate meaningful comparison across predictors, the relative contribution of each feature was calculated as the ratio of its importance score to the sum of all feature importances. This normalized metric reflects the proportional influence of each predictor within the model. Since Scikit-learn's RandomForestRegressor.feature_importances_ provides these values as normalized contribution summing to 1, the output inherently aligns with the relative contribution.~~

2.10 Spatial heterogeneity assessment using GWR

Formatted: Font: 9 pt

Spatial heterogeneity in the influence of FRP, AOD, and other spatial predictors on LST within the intensive fire zone was assessed using Geographically weighted regression (GWR) at 1x1 km^2 grid. GWR is a spatially explicit regression technique designed to quantify how relationships between predictors and a dependent variable vary across geographic space by estimating spatially varying coefficients (Brunsdon et al., 1996). The method applies a distance-based weighting scheme, whereby observations closer to a given location receive higher weights, allowing local parameter estimation that reflects neighbourhood-specific dynamics (Yang et al., 2020). Unlike global regression models that assume spatial stationarity, GWR produces location-specific coefficient estimates, offering a more nuanced understanding of spatially varying associations between LST and its predictors (Fotheringham et al., 2009).~~Spatial heterogeneity in FRP modulated variations in LST across intensive fire zone was further assessed using Geographically Weighted Regression (GWR). It is an advanced statistical method designed to capture heterogeneity in association across space between predictors and dependent variables by constraining spatially-varying coefficient estimates (Brunsdon et al., 1996). The GWR allows regression coefficients to vary locally across geographic space and effectively track these coefficients by using a weight matrix which evaluates the association between kernel and nearby samples (Yang et al., 2020). Unlike global models that assume spatial stationarity, GWR estimates location-specific parameters, thus providing a nuanced understanding of spatially varying relationships between dependent and independent variables (Fotheringham et al., 2009).~~ The GWR model is formally expressed as:

$$y_i = \beta_0(ui, vi) + \sum_{k=1}^{m}(\beta k(ui, vi)\ xik) + \varepsilon i \qquad (6)$$

~~yi = β0(ui, vi) + ∑k=1m βk(ui, vi) xik + εi (6)~~

where (ui, vi) are the coordinates of observation i, βk(ui, vi) are spatially varying coefficients, xik are predictor variables, and εi denotes random error. In GWR, local parameters are estimated using weighted least squares, where each observation is assigned a weight based on its spatial proximity to the location being evaluated. These weights are determined by a spatial kernel function and a bandwidth parameter that defines the extent of spatial influence. Selecting an optimal bandwidth is therefore essential to balance the trade-off between model bias and variance. In this study, the optimal bandwidth was identified through an iterative optimization procedure that minimizes the corrected Akaike Information

Formatted: Superscript

Formatted: Indent: First line: 1.27 cm

Formatted: Font: 9 pt

Criterion (AICc) (Fotheringham et al., 2009). This approach ensures robust estimation of local relationships while effectively accounting for spatial non-stationarity in the dataset. Such a framework is particularly valuable in fire-affected landscapes, where the impacts of fire intensity, aerosol loading, and surface characteristics on LST are inherently heterogeneous and vary substantially across space.~~Here, local parameter is estimated using a weighted least square in which each observation is weighted according to its spatial proximity to the location being evaluated. The weights are determined by a spatial kernel function and a bandwidth parameter, which controls the degree of spatial influence. Choosing an optimal bandwidth is therefore, critical to balance the trade-off between model bias and variance. In this study, the optimal bandwidth is selected through an iterative optimization process that minimizes the corrected Akaike Information Criterion (Fotheringham et al., 2009). This also ensures robust estimation of local relationships while accounting spatial non-stationarity in the dataset.~~

3. Results and discussions

3.1 Spatial association between fire, aerosols and LST

Spatial variations in FRP, LST and AOD averaged for October to November between 2017 and 2021 over extended geographical region is shown in Figure 4(a-c). While residue-based FRP did not exhibit a distinct spatial pattern, temporal variations were prominent, with monthly mean FRP in November (310,188 MW month^{-1}) showing nearly a 100% increase compared to October (152,616 MW month^{-1}; Table S5). In contrast, the spatial pattern of LST exhibited considerable heterogeneity, with relatively higher temperature observed in the southern parts of the region that gradually declined northward. This north–south gradient may be partially attributed to the proximity of the Himalayan foothills, where the cooler mountainous environment likely offsets fire-induced surface warming. A gradual decline in spatially averaged monthly mean LST was also accounted in November (29.0±2.4 °C) compared to October (31.0±1.6 °C). A spatially distinct pattern in columnar aerosol loading was evident across the extended geographical region, with elevated AOD (> 0.65) retrieved over the central areas that gradually decreased towards its periphery (< 0.30). Such spatial variability in aerosol loading is likely driven by differences in the intensity of residue-based fires and the associated emissions of aerosols and trace gas precursors. Moreover, the pronounced increase in monthly mean AOD (October: 0.59 ± 0.08; November: 0.82 ± 0.12)

Formatted: Font: Not Bold

Formatted: Indent: First line: 1.27 cm

Formatted: Font: 9 pt

likely reflects the intensification of fire during early November, compounded by concurrent meteorological influences, most notably the seasonal decline in boundary layer height (Banerjee et al., 2022).

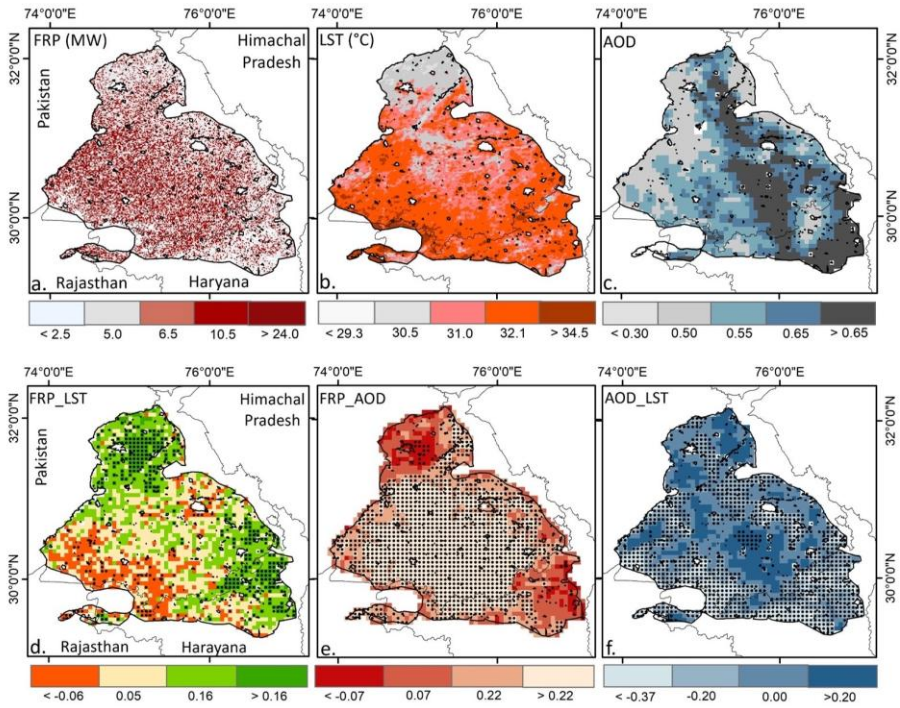

Fig. 4. ~~S~~Spatial ~~association~~ variations of~~between predictor (~~FRP, LST and AOD~~) and dependent variables (LST),~~ over extended geographical region, 5-year mean FRP (a), LST (b) and AOD (c), and spatial correlation between FRP_LST (d), FRP_AOD (e) and AOD_LST (f) ~~over extended geographical region~~. To compute spatial correlation,

~~NOTE. To constitute a spatial association, d~~daily retrievals of FRP, AOD and LST ~~pixels~~ were converted to a common 6x6 km^2 grid. Spatial correlation ~~between FRP, LST and AOD daily retrievals on selected grid~~ was ~~made~~computed for the entire duration ~~over extended geographical region~~and~~. S~~ significant correlation (P<0.05) is shown with black dot.

Formatted: Line spacing: 1.5 lines

Formatted: Font: 12 pt

Formatted: Font color: Text 1

Formatted: Font: 12 pt

Formatted: Superscript

Formatted: Font: 12 pt

Formatted: Font: 12 pt

Formatted: Font: 12 pt

Formatted: Font: 9 pt

Spatial variations in FRP, LST and AOD averaged during for October to November between 2017 and 2021 over extended geographical region without discriminating low to high fire intensity is shown in Figure 4(a-c). While residue-based FRP did not exhibit a distinct spatial pattern, temporal variations were prominent, with monthly mean FRP in November (310,188 MW month^{-1}) showing nearly a 100% increase compared to October (152,616 MW month^{-1}; Table S4). Variations in FRP did not reveal any specific spatial pattern while temporal differences were robust with approximately 100% increase in monthly mean FRP in the month of November (310,188 MW month^{-1}) compared to October month (152,616 MW month^{-1}, Table S3).). In contrast, the spatial pattern of LST exhibited considerable heterogeneity, with relatively higher temperature observed in the southern parts of the region that gradually declined northward.Spatial pattern in LST however, indicate a marked heterogeneity with comparably high temperature at lower southern region that declined gradually towards north. This north–south gradient may be partially attributed to the proximity of the Himalayan foothills, where the cooler mountainous environment likely offsets fire-induced surface warming. A gradual decline in This could potentially due to the proximity of mountainous region which partially offset the fire induced elevated LST in the northern part. spatially averaged monthly mean LST was also accounted in November (29.0±2.4 °C) compared to October (31.0±1.6 °C). Overall, spatially averaged LST monthly mean varied from 28 to 32 °C with slightly higher temperature during October (31.0±1.6 °C) compared to November month (29.0±2.4 °C). On the contrary, a A spatially distinct pattern in columnar aerosol loading was evident across the extended geographical region, with elevated AOD (> 0.65) retrieved over the central areas that gradually decreased towards its periphery (< 0.30). spatially robust signature in columnar aerosol loading was apparent across the extended geographical region. Comparatively high AOD (>0.65) was retrieved at the centre that too receded towards its border (<0.30). Such spatial variability in aerosol loading is likely driven by differences in the intensity of residue-based fires and the associated emissions of aerosols and trace gas precursors. Moreover, the pronounced increase in monthly mean AOD (October: 0.59 ± 0.08; November: 0.82 ± 0.12) likely reflects the intensification of fire during early November, compounded by concurrent meteorological influences, most notably the seasonal decline in boundary layer height. Such spatially robust variation in columnar aerosols potentially influenced by the varying intensities of fire associated emission of aerosols and trace gas precursors. (Banerjee et al., 2022)A strong deviation in monthly mean AOD

Formatted: Font: 9 pt

~~(October: 0.59 ±0.08; November: 0.82±0.12) was also accounted which either influenced by November specific increase in fire intensity and/or meteorological variables, especially due to the decline in planetary boundary layer height (Banerjee et al., 2022).~~

Spatial associations among VIIRS-derived FRP, MODIS LST, and VIIRS-based AOD daily retrievals were assessed over the extended geographical region (Fig. 4d–f). ~~Spatial association between VIIRS FRP against MODIS LST and VIIRS driven AOD daily retrieval was also assessed over pre-identified geographical region (Fig. 4d-f).~~ Spatial correlation between pixel-based FRP against LST reveals positive but ~~a~~ spatially heterogenous ~~positive~~ association across most parts of the study area, except in the southern region~~over major portion of the area except southern part~~. A statistically significant relationship (P < 0.05) between FRP and LST underscores the potential influence of crop residue burning on surface temperature. Similarly, a significant association between FRP and AOD was observed across the central region, where fire intensity was notably higher than in surrounding areas. This spatial covariation between fire intensity and columnar aerosol loading further reinforces the influence of biomass-burning-induced emissions of aerosols and their precursors on atmospheric aerosol abundance. ~~A statistically significant association (P<0.05) between FRP and LST indicates potential influence of crop-based fire on surface temperature. FRP and AOD also accounts a statistically significant association across the central part where fire intensity was considerably high compared to its outskirts. Such spatial covariation between fire intensity and columnar aerosol loading reemphasize the possible influence of incremental aerosols and its precursors' emission from biomass burning on columnar aerosols.~~ Biomass-burning aerosols, predominantly composed of carbonaceous soot particles, are known to modulate the thermal budget of the lower atmosphere (Freychet et al., 2019; Xu et al., 2021). The spatial association between AOD and LST further supports the existence of a fire–aerosol–surface temperature nexus over northwestern India. A comparatively weak yet statistically significant positive correlation between AOD and LST likely reflects lower-atmospheric warming induced by smoke aerosols, consistent with the similar warming effect over western United States during 2017 California wildfire (Gomez et al., 2024).

~~Biomass burning aerosols primarily being carbonaceous smoke particles are reported to modulate lower atmospheric thermal budget (Bond et al., 2013). Spatial association between AOD and LST provide further evidence on possible fire-aerosols-surface temperature~~

Formatted: Font: 9 pt

~~nexus over northwest India. A comparatively low but significant positive association between AOD and LST was possibly the consequence of smoke aerosols induced lower atmospheric warming, as was also accounted by Gomez et al. (2024) over western United States during 2017 California wildfire.~~

3.2 Evaluation of Hurst exponent

The Hurst exponent was evaluated to assess the long-term persistence of fire intensity, surface temperature, and aerosol loading time series over the extended geographical region. In principle, the Hurst exponent is used to quantitatively distinguish a purely stochastic time series (H = 0.50) from a persistent (H > 0.50) or anti-persistent (H < 0.50) time series of pixel-based FRP, LST, and AOD, following the methodology described in Markonis and Koutsoyiannis (2016) and Chen et al. (2022).~~Hurst exponent was evaluated to ascertain long-term persistence of fire intensity, surface temperature and aerosol loading time-series over the intensive fire zone. Principally, Hurst exponent is employed to quantitative segregate a stochastic time series (H: 0.50) against a sustainable (H> 0.50) and anti-persistence time series (H< 0.50) of pixel-based FRP, LST and AOD following the protocol as mentioned in Markonis and Koutsoyiannis (2016) and Chen et al. (2022).~~

As shown in Figure 5, nearly the entire extended geographical region of northwestern India exhibits Hurst exponent values greater than 0.50 for FRP, with relatively higher values (0.60–0.70) concentrated toward its central zone. Although variations in Hurst exponent for FRP was spatially inconsistent, primarily due to temporal and spatial fluctuations in fire intensity, the FRP time series over most of the region indicates statistical persistence. Similarly, elevated Hurst exponent values for LST (>0.50) across the region also exhibits persistence at long run. Notably, the northern portion of the study region shows slightly higher Hurst exponent values compared to the southern part. For regional aerosol loading, except few isolated patches, comparatively high Hurst exponent values (>0.75) were observed over the central region. Notably, this area also coincides with zones characterized by high AOD (>0.65) and a statistically significant FRP–AOD association. Overall, the Hurst exponent analysis indicates that the observed FRP, LST, and AOD time series across most of the residue-burning region exhibit statistical persistence.

Formatted: Indent: First line: 1.27 cm

Formatted: Font: 9 pt

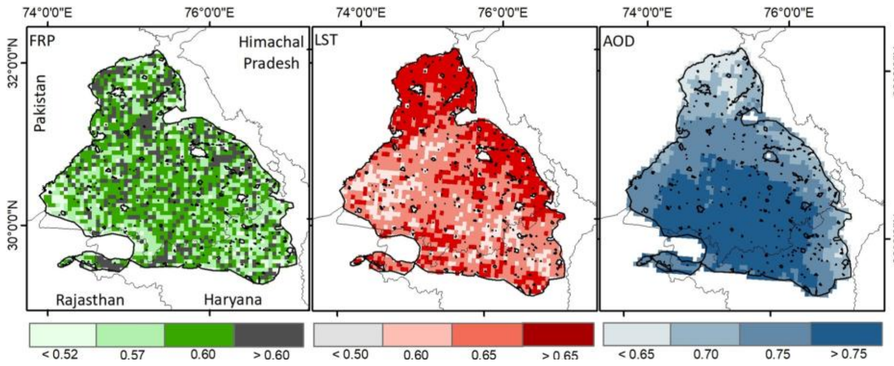

Fig. 5. Estimating FRP (MW), LST (°C) and AOD time-series persistence in extended geographical region~~-~~.

~~It could be seen from Fig. 5 that almost entire 'extended geographical region' over northwest India appears to have a Hurst exponent >0.50 for FRP with relatively high exponent (0.60-0.70) at the centre. Although the variations in Hurst exponent was not highly consistent as fire intensity fluctuates with time and space, we note that the accounted FRP time-series over major proportion of the region should sustain in longer time period. Similarly, a high exponent for LST (>0.50) across the region entails LST time-series too persisted and possibly remain stable in near future. For agriculture land located at the northern part, Hurst exponent appeared to be >0.65 indicating a strong trend in LST time series. For regional aerosol loading, barring few isolated tiny patches, Hurst exponent enhanced with space and time and accounted highest value (>0.75) over the central part. The region also coincides with area having high AOD (>0.65) and statistically significant association for FRP and AOD.~~

However, interpretation of the Hurst exponent results should be approached with caution. The five-year dataset used here may not be sufficient to derive statistically robust estimates. For the same reason, trend analysis was not undertaken, as the limited dataset constrains the reliability of such estimates and falls beyond the scope of the present study. Nonetheless, several studies have documented long-term trends in fire dynamics and aerosol loading over northwestern India ~~It is noteworthy that trend analysis was not undertaken, as such estimation falls beyond the scope of the present study. Moreover, the five-year dataset may not be sufficient to derive statistically robust trends comparable with previous long-term~~

Formatted: Left, Indent: Left: 0.25 cm, Hanging: 1.25 cm, Space Before: 0 pt, After: 0 pt, Line spacing: 1.5 lines

Formatted: Indent: Left: 0.25 cm, Hanging: 1.25 cm

Formatted: Font: 9 pt

~~assessments. Nonetheless, several studies have documented long-term trends in fire dynamics and aerosol loading over northwestern India~~ (e.g., Vadrevu and Lasko, 2018; Jethva et al., 2019; Singh et al., 2020).~~Its noteworthy that we have avoided analysing trend in respective time series as such estimation was not within the scope of the present research. Besides, a 5-year time period may not result statistically robust trend deemed comparable with previous estimates. Long-term trend in fire dynamics and aerosol loading over the northwest region has however been reported by several researches, like Vadrevu and Lasko (2018), Jethva et al. (2019) and Singh et al. (2020).~~

3.3 Surface temperature and aerosols response to fire intensity

Fire intensity in terms of pixel-based FRP, aerosol loading and surface temperature were retrieved to ~~constitute~~ compute corresponding ~~respective~~ daily ~~means~~ and spatial means based on five years of satellite retrievals. It is noteworthy that to account immediate response of fire intensity and aerosol loading on surface temperature, all variables were retrieved exclusively over year-specific ~~-wise~~ intensive fire zones, having cumulative FRP ≥ 5 MW grid^{-1}~~.~~, as illustrated in Fig. 2(b-f).

Formatted: Font: 9 pt

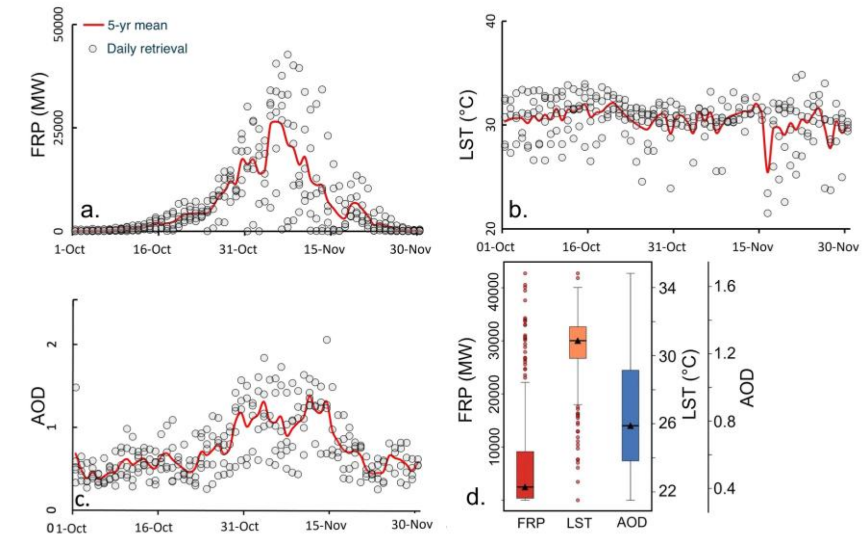

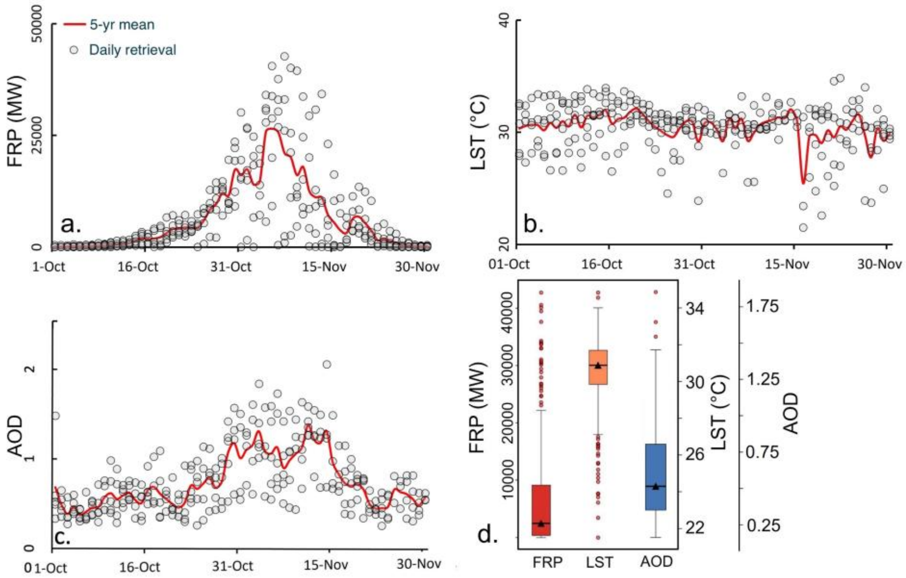

Fig. 6. Time series of five-year mean fire radiative power (FRP, a), land surface temperature (LST, b) and aerosol optical depth (AOD, c) against daily retrievals, (d) covariation of FRP, AOD and LST over intensive fire zone.

Gray dots show daily retrievals from October to November (2017–2021), with the red line depicting the corresponding 5-year mean.~~NOTE: Gray dots indicate daily retrievals from~~

Formatted: Line spacing: 1.5 lines

Formatted: Font: 9 pt

~~October to November over the years from 2017 to 2021 while 5-yr mean is the daily average based on retrievals from 2017 to 2021, and is indicated with red line.~~

A distinct temporal pattern is evident in the FRP time series (Fig. 6a), which corresponds closely with daily variations in fire counts (Fig. S4). Over northwestern India, FRP starts to build-up typically in mid-October, peaks consistently during the first week of November, and declines thereafter by mid-November. In contrast, the temporal pattern of the five-year mean LST time series appears less pronounced, as daily retrievals exhibit substantial variability. Regional LST demonstrates both interannual and intra-annual fluctuations, as illustrated in Fig. S5. Notably, the FRP time series aligns well with the mean columnar aerosol loading, underscoring the potential influence of aerosol and precursor emissions from widespread biomass burning.~~A robust temporal pattern could be extracted from FRP timeseries (Fig. 6a) which reciprocates well with corresponding daily variations in fire count (Fig. S3). We note FRP initiates during mid-October over northwest India and reaches its peak consistently in the first week of November before reducing mid-November onwards. In contrast, temporal pattern in five-year mean LST timeseries is less intensive as daily retrievals shows extensive range of deviations. Regional LST clearly reflects both inter- and intraannual fluctuations, as shown in Fig. S4. FRP time series however, matches well with mean columnar aerosol loading emphasizing possible effect of emission of aerosols and its precursors from extensive biomass burning. The characteristic rise in AOD during first two weeks of November possibly exhibits the direct response to elevated fire intensity as columnar aerosols consistently surpass 1.00 over the intensive fire zone. Interestingly, every year in between October 25 to November 20, 90% of daily AOD exceeds 5-yr mean AOD (0.74±0.28) with corresponding 800% rise in average FRP (13085±6825 MW) compared to rest of the period (1148±1478 MW). Dring this interlude, five-year mean columnar AOD corelates well with 5-yr aggregate FRP (r: 0.46) and mean LST (0.41) which was otherwise, not the case for the remaining period (AOD-FRP: 0.18; AOD-LST: -0.02).~~

The characteristic rise in AOD during the first two weeks of November likely represents a direct response to intensified fire activity, as columnar AOD values consistently exceed 1.00 over the intensive fire zone. Interestingly, between October 25 and November 20 each year, approximately 90% of daily AOD observations surpass the five-year mean (0.74 ± 0.28),

Formatted: Indent: First line: 1 cm

Formatted: Font: 9 pt

coinciding with an 800% increase in average FRP (13,085 ± 6,825 MW) compared to the remainder of the season (1,148 ± 1,478 MW). During this interval, the five-year mean columnar AOD exhibits a strong association with the aggregate FRP (r = 0.46) and mean LST (r = 0.41), whereas these associations weaken considerably outside this period (AOD–FRP: r = 0.18; AOD–LST: r = –0.02).

The temporal associations among FRP, AOD, and LST clearly demonstrate the immediate response of fire-induced variations in aerosol loading and surface temperature over northwestern India. Accordingly, in the subsequent section, these relationships were ~~modeled~~modelled using a geospatial tree-based regression framework that integrates concurrent temporal features (e.g., day-specific retrievals) and spatial predictors (e.g., regional meteorology, aerosol loading, and fire intensity) to quantify and characterize the FRP–AOD–LST nexus within the intensive fire zone.~~Temporal association between FRP-AOD and LST clearly illustrates the immediate response of fire-associated changes in aerosol loading and surface temperature over the northwest part of India. In the subsequent section, such association was therefore, modelled using a geospatial tree-based regression model using several concurrent temporal (like day-specific retrieval) and spatial features (like regional meteorology, aerosol loading and fire intensity) to construct FRP-AOD-LST nexus over intensive fire zone in northwest India.~~

3.4 Fire induced change in LST and AOD

The effect of crop residue burning on land surface temperature and aerosol loading was assessed ~~Crop residue burning–induced changes in surface temperature and aerosol loading were quantified~~ using a space-for-time ~~substitution~~ approach by overlaying grid-based VIIRS LST, FRP, and AOD datasets over the northwestern region experiencing recurrent fire. To remove potential confounding effect, ~~F~~fire and no-fire grids were retained for comparison only when they matched in terms of topography, meteorology, physical environment, vegetation and soil characteristics, climatological mean LST and AOD, and surface property. Comparisons were performed within defined strata containing grids with identical characteristics to ensure that the quantified changes in LST and AOD ~~could be~~could be attributed solely to fire~~ activity~~. A total of ~~600~~7489 paired no-fire and fire grids were used between 2017 and 2021 to quantify the relative change in LST and AOD. It is noteworthy that

Formatted: Font: 9 pt

all grids, whether exhibiting fire or not, were selected from within the extended geographical region to capture localized variations in temperature and aerosol loading.

~~Crop-residue based fire induced changes in surface temperature and aerosol loading wereas quantified using space-for-time approach, by overlaying grid-based VIIRS LST, FRP and AOD at 10x10 km^2 resolution over year-specific intensive fire zone. As illustrated in Fig. 7, and supported by the year-specific datasets summarized in Table S5with year-specific dataset included in Table S4, a clear and robust pattern of change in LST and AOD was noted over the areas exhibiting affected by residue-based fire against that of no fire zone. The results are presented in terms of anomalies, where positive (negative) LST values indicate regional warming (cooling). Results are reported in terms of anomaly where a positive (negative) ΔLST indicates reginal warming (cooling). Fire activity induced an average increase of 0.48 °C in LST across fire-affected zones during 2017–2021, with notable temporal variability ranging from –0.55 °C to 1.69 °C. Fire induced an increase in LST by 0.48 °C over the fire zone during year 2017 to 2021, with marked temporal heterogeneity in temperature change with a range varying from -0.55 to 1.69 °C. It impliesy that there was instance when fire had cooling effect on surface temperature, as was in year 2019, although a very limited number of grid (2) exhibiting no fire could possibly the reason behind such unanticipated result. Barring this, an increase in LST was accounted in each year averaging 0.72 °C year^{-1} which could possibly due to reduced evapotranspiration, as was also noted reported during forest fire (Liu et al., 2018, 2019). Similarly, Zhang et al. (2020) asserted an increase in LST by 1-3 °C by agriculture residue-based fire in three provinces across China.Results reported in this study are consistent with the findings of Liu et al. (2019), who attributed a 0.15 K rise in surface temperature over burned areas globally to satellite-observed forest fires, as well as with Liu et al. (2018), who reported a net warming effect over the Siberian boreal forest. Additional evidence from studies such as Alkama and Cescatti (2016) and Zhao et al. (2024) also indicates a positive linkage between forest fire incidence and intensity with surface temperature. However, the biophysical effects of agricultural residue burning on land surface temperature remain observationally limited, making it challenging to constrain its environmental consequences across diverse landforms. In a recent study, Zhang et al. (2020) reported elevated LST by 1-3 °C over three provinces in China associated with crop residue~~

Formatted: Indent: First line: 1.27 cm

Formatted: Font: 9 pt

~~burning. Nevertheless, the feedback effect of air temperature on fire occurrence was not considered.~~

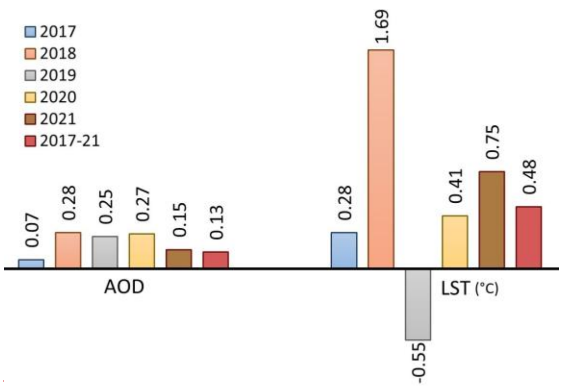

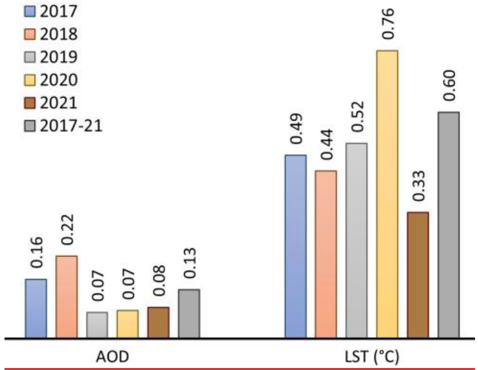

Fig. 7. Crop-residue-based fire induced changes in ~~LST~~ land surface temperature and aerosol loading~~AOD over intensive fire zone.~~.

As illustrated in Fig. 7, ~~, with year specific datasets summarized in Table S5,~~ a consistent yet temporally dynamic increase in both LST and AOD was observed over regions affected by residue-based burning compared with no-fire zone. However, the magnitude of LST and AOD change across the fire zone was spatially heterogeneous. On average, residue-based burning induced an increase of 0.60 °C in LST during 2017–2021, with interannual variability ranging from 0.33 °C to 0.76 °C. This indicates that residue burning exerts a persistent warming influence on land surface temperature, likely driven by reduced evapotranspiration, enhanced shortwave absorption, increased sensible heat flux, and fire-induced changes in surface albedo. However, a strong spatial heterogeneity in LST and AOD

Formatted: Font: Not Bold

Formatted: Font: Not Bold

Formatted: Font: Not Bold

Formatted: Centered, Space Before: 0 pt

Formatted: Indent: First line: 1.27 cm

Formatted: Font: 9 pt

modulation further indicates the potential influence of key confounding factors and intensity of fire in regulating the change. ~~As illustrated in Fig. 7 with year-specific datasets summarized in Table S5, a consistent pattern of change in LST and AOD was noted over the areas affected by residue-based fire against that of no-fire zone. Fire activity induced an average increase of 0.60 °C in LST across fire-affected zones during 2017–2021, with notable temporal variability ranging from 0.33 °C to 0.76 °C. It implies that fire had a consistent warming effect on surface temperature which could possibly due to reduced evapotranspiration and fire-induced changes in surface albedo, as was also reported during forest fire.~~

~~T~~The results of this study align with Liu et al. (2019), ~~he results reported in this study are consistent with those of Liu et al. (2019), ~~who attributed a 0.15 °C rise in surface temperature over burned areas globally to satellite-observed forest fires, as well as Liu et al. (2018), who documented a net warming effect over the Siberian boreal forest. Additional evidence from Alkama and Cescatti (2016) and Zhao et al. (2024) also indicates a positive linkage between forest fire occurrence, ~~and~~ fire intensity, ~~with~~and surface temperature. In contrast, the biophysical effects of agricultural residue burning on land surface temperature remain poorly constrained. ~~However, the biophysical effects of agricultural residue burning on land surface temperature remain observationally limited, making it difficult to constrain its environmental consequences across diverse landforms. In a recent study, Zhang et al. (2020) reported elevated LST by 1–3 °C over three provinces in China associated with crop residue burning; however, the feedback effect of air temperature on fire occurrence was not considered.~~Zhang et al. (2020) reported LST increases of 1–3 °C over three provinces in China associated with crop residue burning. However, the feedback effects of meteorological covariates and systematic land-cover differences on fire occurrence were not accounted for, leading to causal attribution of fire to LST remains tentative.

Formatted: Indent: First line: 1.27 cm

A consistent annual increase in aerosol loading was also observed over the fire-affected grids over northwestern India~~ affected by fire compared to non-fire grids~~. ~~Satellite-based observations revealed a~~A clear upward trend in AOD was noted ~~within~~across the fire

Formatted: Font: 9 pt

zones, with a mean increase of 0.13 AOD year^{-1} and a range of 0.07–0.22 AOD year^{-1}. ~~Notably, this~~The ~~increase~~change in columnar aerosol loading, however, was spatially heterogeneous~~AOD persisted throughout the monitoring period~~. Overall, the increase in AOD from fire-associated emissions of aerosols and their gaseous precursors reinforces the source-specific contribution of crop residue burning, a phenomenon well documented in previous studies (Vinjamuri et al., 2020; Mhawish et al., 2022).~~Overall, the increase in AOD from fire-associated emissions of aerosols and their gaseous precursors reinforces the source-specific contribution of crop residue burning, a phenomenon well documented in previous studies Vinjamuri et al., 2020; A consistent increase in aerosol loading was also observed over grids affected by fire compared to non-fire zones. Satellite-based observations revealed a clear upward trend in AOD over the fire zones, with a mean increase of 0.19 AOD year~~$^{-1}$ ~~and a range of 0.07–0.28 AOD year~~$^{-1}$~~. Notably, this increase in AOD remained consistent throughout the monitoring period, reinforcing the link between biomass burning emissions and elevated aerosol concentrations over the source regions, a relationship well-documented in previous global studies (Mhawish et al., 2022).A consistent increase in aerosol loading was also accounted over the grids encountered with fire against no fire zone. Satellite based observation shows a clear trend in increasing AOD over the fire zone with a mean rise of 0.19 AOD year-1 with a range 0.07 to 0.28 AOD year-1. Interestingly, increase in AOD was consistent across the monitoring period which link biomass burning emission with elevated aerosol emission over the source region, reported in literature across the globe (Mhawish et al., 2022; Ravindra et al., 2023).~~

To quantify uncertainty in the estimated differences between fire-affected and non-fire-affected grid cells, we further computed 95% confidence intervals for ΔLST and ΔAOD using nonparametric bootstrapping. For each variable, 10,000 bootstrap samples were generated by resampling grid cells with replacement, and the mean difference was recalculated for each bootstrap replicate. The 2.5th and 97.5th percentiles of the resulting sampling distribution were taken as the bounds of the 95% confidence interval (CI). Nonparametric bootstrapping results into significant increase in both ΔLST (0.57°C; 95% CI: 0.33–0.81°C) and ΔAOD (0.13; 95% CI: 0.08–0.17) in fire-affected regions. Because both CIs do not overlap zero, these differences are statistically robust and unlikely to be due to sampling variability.

Formatted: Font: (Default) +Body (Calibri), 12 pt, Font color: Auto

Formatted: Indent: First line: 1.27 cm

Formatted: Font: (Default) +Body (Calibri), 12 pt, Font color: Auto

Formatted: Superscript

Formatted: Font: (Default) +Body (Calibri), 12 pt, Font color: Auto

Formatted: Superscript

Formatted: Font: (Default) +Body (Calibri), 12 pt, Font color: Auto

Formatted: Font: (Default) +Body (Calibri), 12 pt, Font color: Auto

Formatted: Font: (Default) +Body (Calibri), 12 pt, Font color: Auto

Formatted: Font: Not Bold, Font color: Auto

Formatted: Font: 9 pt

3.5 Spatial regression of fire intensity and aerosols on LST

A machine learning algorithm was employed to establish the statistical association between the dependent variable LST and multiple predictors including~~,~~ fire radiative power, aerosol loading, regional meteorology (Fig. S6), surface properties, and vegetation characteristics~~, and the dependent variable LST~~. ~~Relative feature importance (RFI) of all predictors was first evaluated for the fire season, and the marginal effects of FRP and aerosols on LST were subsequently quantified.~~ All ~~B~~biophysical parameters, except SR and soil moisture, retrieved under two pre-defined scenarios, (one) days with moderate-to-high fire intensity and (two) days with sustained high fire intensity exhibiting a positive association with regional mean LST, were used to model the FRP–AOD–LST relation.~~To establish a possible association between predictors *viz*. fire intensity, aerosols and meteorology on dependent variable LST, a machine learning algorithm was employed hypothesizing non-linear statistical association among the variables. The choice of Random Forest (RF) to regress the association was based on its excellent accuracy, ability to handle large dataset, superior performance and prior applications on LST-based research (Logan et al., 2020; Wang et al., 2022; Zhang et al., 2025). Here, relative importance of fire intensity, aerosol loading and meteorological variables (Fig. S5~~S6) were assessed to sustain spatial variations in LST across the year-constrained intensive fire zone. Further, relative contributions of each predictors were quantified and marginal effects of predictor variables on LST have been quantified. Two pre-specified scenarios (Table ~~S5~~S6), one, that includes days with extended fire intensity starting from fire initiation to terminate, and second, days including high intensity fire having strong positive correlation between FRP and LST were modelled. Such approximation were meant to evaluate and compare the relative importance of predictor variables both in the cases of high intensity fire and during entire crop-based fire episode.~~

Relative feature importance (RFI) of ~~all~~selected predictors was first evaluated for the fire season, and the marginal effects of FRP and aerosols on LST were subsequently quantified. Figure 8(a) presents the normalized RFI values for all predictors under both scenarios, and the Random Forest hyperparameter tuning procedure is summarized in Table S6. ~~Figure 8(a) illustrates the normalized RFI of the predictors across the two scenarios.~~ RFI quantifies the sensitivity of regional LST to each predictor and reflects their partial contribution to surface temperature variability. Fire radiative power emerged as the

Formatted: Justified, Indent: First line: 1.25 cm

Formatted: Font: 9 pt

dominant predictor under both scenarios, indicating the strong influence of fire-related energy release on regional radiative balance, likely through reduced evapotranspiration and fire-induced changes in surface albedo (Liu et al., 2018, 2019). Notably, the RFI was substantially higher during period of sustained high-intensity burning (Scenario 2; RFI = 0.40) compared with days characterized by moderate-to-high fire activity (Scenario 1; RFI = 0.22), highlighting the stronger thermal response associated with intensive burning condition.

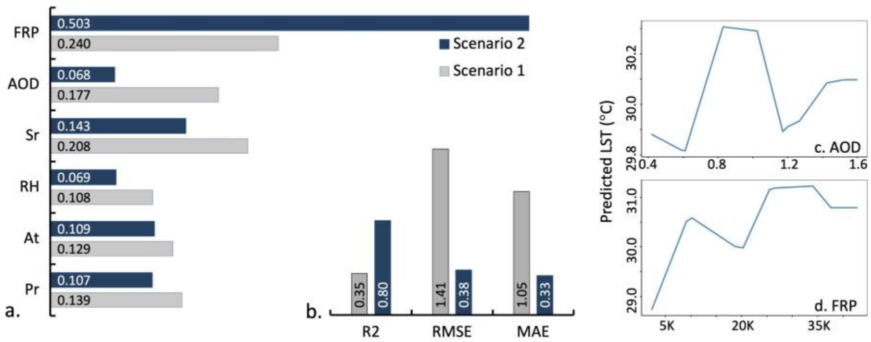

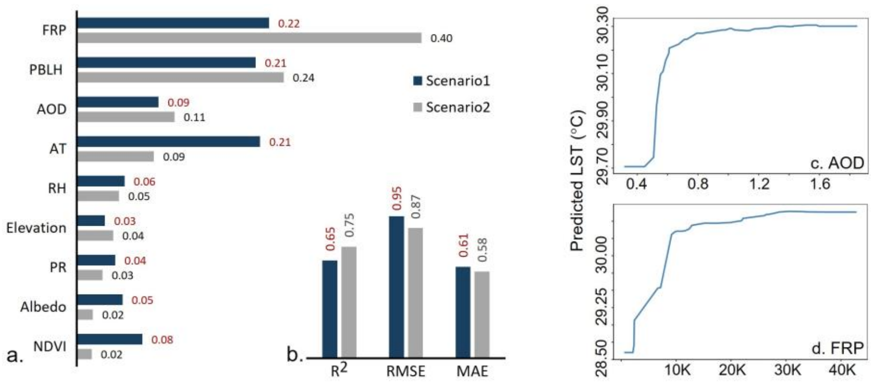

Fig. 8. Normalized r ~~R~~elative feature importance of predictor variables on LST (a), ~~statistical~~ cross-validated evaluation of ~~performance of~~ random forest performance ~~for two diverse scenarios~~ (b), and partial dependence plots of LST on AOD (c) and FRP (d).

~~NOTE. For Fig. 8d,~~Here, K indicates x1000. The PDP plots are based on scenario 2. Both RMSE and MAE have unit °C.

Formatted: Indent: Left: 0 cm, Hanging: 1.28 cm

Formatted: Font: 12 pt

Formatted: Indent: Left: 0 cm, Hanging: 1.28 cm, Space Before: 6 pt, After: 6 pt, Line spacing: 1.5 lines

Formatted: Font: 12 pt

Formatted: Font color: Auto

Formatted: Font: (Default) +Body (Calibri), Font color: Auto

Formatted: Indent: Left: 0 cm, First line: 1.25 cm

Formatted: Font: 9 pt

~~Figure 8(a) indicate the relative feature importance (RFI) of the selected predictor variables modelled across the identified scenariossl regional~~Next to FRP, PBLH exerted a significant influence on LST (RFI: 0.21–0.24), followed by atmospheric temperature (RFI: 0.09–0.21). The strong effect of PBLH on LST can be explained by restricted turbulent mixing during shallow boundary-layer conditions in post-monsoon season. A relatively low PBLH (mean±SD: 71±29 m) over northwestern India reduces vertical mixing and traps fire-induced heat and aerosols close to the surface (Vinjamuri et al., 2020). This enhances shortwave absorption, suppresses evaporative cooling, and limits turbulent heat dissipation, resulting in a stronger and more persistent increase in LST. Another notable finding was the modification of LST due to enhanced columnar aerosol loading during fire season. The RFI of AOD varies from 0.09 to 0.11, indicating its influence on regional radiative budget. Residue burning releases aerosols and their gaseous precursors, which can exert significant radiative impacts and drive rapid adjustments in both surface and atmospheric temperature (Freychet et al., 2019; Xu et al., 2021). Fire-generated aerosols influence the energy balance through scattering and absorption of radiation, alterations in cloud microphysics, and changes in surface albedo via deposition of carbonaceous particles. However, the magnitude and direction of these radiative effects remain uncertain at the global scale (Tian et al., 2022).

The partial influence of all other parameters, including meteorological variables, ~~soil and~~ land characteristics and elevation was less significant (RFI < 0.30).

~~. Variable relative feature importance refers the sensitivity of LST against individual predictors and serves as an identity about their partial influence in predicting LST. Scenario 1 resulted the strongest influence of FRP (RFI: 0.240) on LST across the intensive fire zone followed by solar radiation (0.208) and aerosol loading (0.177). The partial influence of other parameters including meteorological variables were less significant (<0.140).~~

~~Interestingly, FRP also emerged as the top feature in modulating LST variation during scenario 2 with robust RFI of 0.503. This essentially establish the added contribution of excessive heat energy released during high intensity fire on LST modifications over high intensity residue-based fire zone. The very next contribution on LST variations was due to SR (RFI: 0.143) and aerosol loading (RFI: 0.068) which emerged to reduce significantly against scenario 1 when fire intensity spread across over extended time period.~~

Formatted: Indent: First line: 0 cm

Formatted: Underline

Formatted: Font: 9 pt

~~The prediction of FRP as the top feature to modulate LST changes during crop residue-based fire event is imperative as it hold greater repercussion on the regional climate and human health. However, the RFI scores for both FRP and SR were comparable indicating their shared partial influence on LST. Another interesting finding was to attain significant impact of columnar aerosol loading on LST modification which was otherwise reported by researchers investigating global fire aerosols and climate (Tian et al., 2022).~~

~~It is noteworthy that RF model performance for the scenario 1 records high RMSE (1.41 °C) and MAE (1.05 °C) with comparatively low R^2 (0.35) which translates into some uncertainties in the prediction.~~

~~In contrast, a superior model performance was achieved in case of scenario 2 when very high coefficient of determination (R^2: 0.80) was accounted with sufficiently less RMSE (0.38 °C) and MAE (0.33 °C). This ensured a robust model prediction when high correlation coefficient between FRP and LST were selectively considered.~~ The predictive skill of the random forest model was assessed using temporal block cross-validation to minimize temporal autocorrelation and prevent data leakage. Under both scenarios model performance was found satisfactory with R^2 varying from 0.65-0.75, marked with relatively low RMSE (0.87-0.95 °C) and MAE (0.58-0.61 °C). A satisfactory model performance also ensures that residue burning provide a clear LST response and the RF model was able to resolve non-linear land–atmosphere interactions, irrespective of the selected scenarios. R~~A~~ ~~r~~elatively better performance was however, achieved ~~during~~in scenario 2 during the fire days having better spatial association between FRP and LST. Collectively, this confirms that moderate-to-high intensity residue burning leaves a measurable and predictable thermal signature on the land surface over northwestern India.

~~Interestingly, FRP also emerged as the top feature in modulating LST variation during scenario 2 with robust RFI of 0.503. This essentially establish the added contribution of excessive heat energy released during high intensity fire on LST modifications over high intensity residue-based fire zone. The very next contribution on LST variations was due to SR (RFI: 0.143) and aerosol loading (RFI: 0.68) which emerged to reduce significantly against scenario 1 when fire intensity spread across over extended time period.~~

Formatted: Indent: First line: 0 cm

Formatted: Superscript

Formatted: Font: 9 pt

The partial dependence plots (PDPs) in Fig. 8(c–d) illustrate the marginal effects of FRP and AOD on LST. These plots show the expected change in LST associated with variation in each predictor while holding all other predictors constant. The estimated effects of both FRP and AOD exhibit a non-linear, saturating response. LST increases sharply at low-to-moderate values of each predictor but the effect progressively weakens at higher magnitudes, approaching an asymptotic limit. This behaviour likely arises from the complex interplay of radiative and thermodynamic processes associated with biomass-burning emissions. Fire-originated aerosols exert both direct and indirect radiative effects whose magnitudes and signs vary with aerosol loading and composition (Freychet et al., 2019; Xu et al., 2021; Tian et al., 2022). ~~The partial dependence plots (PDPs) illustrating the marginal effects of FRP and AOD on LST are presented in Fig. 8(c–d). These plots depict the relative change in LST associated with a unit change in each predictor variable, while keeping other predictors as constant. The estimated effect of AOD on LST appears non-linear, characterized by an abrupt reversal in trend when AOD range between 1.00 and 1.20. The non-linear association between fire-originated aerosols and regional LST likely arise from the complex interplay of multiple radiative and thermodynamic processes. Fire-emitted aerosols may exert both direct and indirect radiative effects that vary in magnitude and direction (Bond et al., 2013; Li et al., 2016).~~ At moderate aerosol loading, UV-absorbing black carbon aerosols may enhance atmospheric heating and can transiently increase near-surface temperature (Jacobson, 2001). Fire-induced convective plumes may initially enhance surface temperatures, whereas strong aerosol build-up can reduce solar transmittance to the ground. Aerosol–cloud interactions further contribute to non-linearity by modifying cloud microphysics, lifetime, and albedo, altering the regional radiative balance. Additionally, aerosol-driven changes in boundary-layer structure, evapotranspiration, and soil moisture introduce additional land–atmosphere feedbacks. Together, these interacting processes operate across multiple spatial and temporal scales and do not scale linearly with aerosol loading or fire intensity, producing the observed non-linear LST response. The RF model therefore provides strong evidence that both fire intensity and fire-derived aerosols exert measurable and non-linear effects on regional LST, with potentially important implications for the regional radiative budget. ~~Alternatively, once sufficient aerosols build-up from fire, strong attenuation of shortwave radiation substantially declines net LST (Eck et al., 2010). Moreover, fire induced convective plumes may initially increase surface temperature while at high aerosol build-up situation~~

Formatted: Font: 9 pt

~~may suppresses solar transmittance to surface. Aerosol–cloud interactions further contribute to this non-linearity by modifying cloud microphysics, lifetime, and albedo, thereby altering the regional radiation balance (Rosenfeld et al., 2019). Furthermore, aerosol-induced changes in boundary layer, evapotranspiration, and soil moisture create additional land–atmosphere feedbacks. Collectively, these interdependent processes operate across multiple spatial and temporal scales and do not scale linearly with aerosol loading or fire intensity, leading to the observed non-linear LST response in crop residue burning regions. In contrast, the marginal effect of FRP on LST is more consistent, showing a pronounced positive association in which increases in regional FRP correspond to higher LST for all observed conditions.The partial dependence plot (PDP) on the marginal effects of FRP and AOD on LST have been included in Fig. 8(c-d). This indicates the relative change in LST with corresponding unit change in predictor variable when other predictors remain stable. The effect estimates of unit increase in AOD on LST remained inconsistent because of sudden reversal of trend when AOD remain within 1.00 to 1.20. In contrast, the marginal effect of FRP on LST has been prominent with an increase in regional FRP resulted in consequent increase in LST for almost all the cases. TThe RF model thus provides robust evidence on the effects of crop residue–based fire energy and aerosol emissions on regional LST, which may have wide-ranging implications for regional radiative budget.~~

~~he RF model therefore, concludes with certainty the implications of crop-residue based fire associated release of energy and aerosols on regional LST which could have diverse consequences on regional climate, agriculture and human health.~~

3.6 Geographically weighted regression on LST

A Global Moran's I test was first applied to assess spatial autocorrelation in LST across the intensive fire zone for the cumulative five-year period. As shown in Table S6, Moran's I was 0.225, accompanied by a high positive Z-score and a statistically significant p-value (< 0.001), indicating a clustered spatial pattern of LST that is highly unlikely ($<1\%$) to have arisen by random chance. Given this spatial dependence, GWR was employed to evaluate spatial heterogeneity in the relationships between LST, FRP, and other predictors. All variables used in the Random Forest model were incorporated into the GWR framework under both pre-defined scenarios. Model specifications and performance metrics including bandwidth and kernel details are mentioned in Table S8.

Formatted: Justified, Indent: First line: 1.27 cm

Formatted: Font: 9 pt

~~Initially, Global Moran' I test was performed to verify spatial autocorrelation in LST across the intensive fire zone cumulatively for five years. Results, as in Table S6~~S7~~, indicate Moran'I value (0.224) for LST has a high positive Z-score and remain spatially significant (p-value: 0.000). This refers very less possibility (<1%) of the clustered LST pattern could be due to random chance. Therefore, geographically weighted regression (GWR) was performed to assess spatial heterogeneity in FRP driven variations on LST across year-specific intensive fire zone over northwest~~ern~~ India. GWR was however, simulated only for the main predictor FRP against dependent LST for scenario 2 based on prior outcome from RF regression. Figure 9 details the spatial outcome of GWR for the entire duration while model running criteria and year-wise performance is included in Table S7~~S8~~. Results indicate spatial heterogeneity in coefficient estimates with overall positive values over the intensive fire zone. It was however, predictable as FRP over the intensive fire zone did vary with time and space which potentially influence LST at a diverse scale. Overall, GWR model clearly imply that higher FRP is primarily associated with increase in LST over the region which potentially have implications on regional climate and agriculture.~~

Formatted: Font: 9 pt

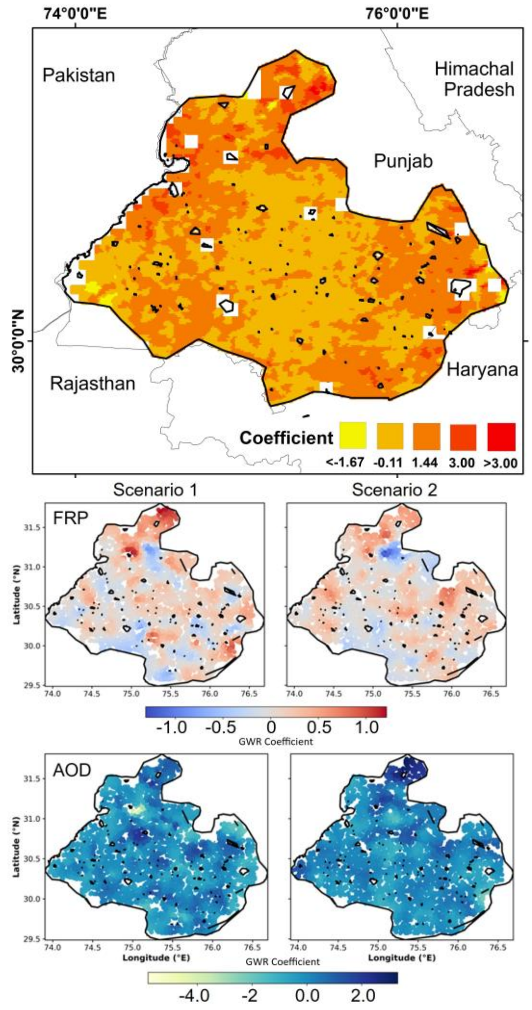

Fig. 9. Spatial distribution of FRP and AOD GWR coefficients across intensive fire zone.

GWR model demonstrated strong explanatory power, with global R^2 values exceeding 0.74, confirming that the selected predictors effectively captured spatial variability in LST. FRP consistently showed a positive and spatially varying association with LST across both scenarios, underscoring its dominant influence in fire-affected regions. Aerosol loading demonstrated weak but spatially heterogeneous effects, reflecting localized differences in aerosol–temperature interactions. Other predictors, including NDVI, RH, AT, PBLH, elevation,

Formatted: Space Before: 6 pt

Formatted: Font: Not Bold

Formatted: Indent: First line: 1.27 cm

Formatted: Font: Not Bold

Formatted: Font: 9 pt

and albedo (Fig. S7), exhibited local coefficients ranging from −0.76 to +0.23, indicating spatial variability but comparatively weaker contributions to LST modulation across the study area.

Conclusions

~~This analysis reveals that physical effect of crop-residue-based fire can substantially affect the regional climate by modifying land surface temperature over an extensive geographical region in northwest India. However, the magnitude of surface temperature modification could vary with intensity of fire and associated modulation by regional meteorology. Results reported here were in line with the findings of Liu et al. (2019) when satellite-based observations on forest fire was held accountable for 0.15 K rise in surface temperature over burned area globally, and a net warming over Siberian Boreal Forest (Liu et al. (2018). There are other evidences too, as in Alkama and Cascatti (2016), Zhao et al. (2024) when incidences and intensities of forest fire were positively linked with temperature. However, biophysical effects of agriculturale residue-based fire on land surface temperature are observationally scarce, making it difficult to constrain its environmental consequences over diverse landforms. In a recent work, Zhang et al. (2020) has found association of elevated land surface temperature over three different provinces in China due to crop residual burning. However, feedback of air temperature on fire incidences were not included for consideration. Our effort in understanding residue-based fire associated changes in surface temperature was therefore, novel considering the extensive and recurrent fire incidences over northern India that has been associated with deteriorating air quality in Delhi and its surroundings. The findings of this study are however, limited with inability to measure counter feedback of the agriculture system towards limiting changes in land surface temperature, uncertainty associated with estimating fire radiative power, and accounting aerosols counter feedback on local meteorology and vice-versa.~~

The manuscript unfolds by identifying the geospatial variations in crop residue–based fires and their associated impacts on aerosol loading and land surface temperature across northwestern India. Based on year-wise, pixel-level fire intensity, the geographical region with intensive fire activity was initially delineated, and all satellite-derived and reanalysis datasets were subsequently processed exclusively over the selected zone. A robust and consistent spatial correlation between FRP, AOD, and LST was observed across multiple years, indicating potential fire-induced perturbations in LST. The Hurst exponent analysis reaffirmed the long-

Formatted: Font: 9 pt

term persistence of fire intensity, surface temperature, and aerosol loading time series. A grid-based analysis over the intensive fire zone revealed a significant increase in both LST and AOD during the peak fire season.~~ The manuscript unfolds with identifying geospatial variations in crop residue-based fire, associated aerosol loading and land surface temperature over northern part of India. Based on year wise pixel-based fire intensity, geographical region encompassing intensive fire was earmarked and all satellite-based retrievals and reanalysis datasets were processed only over the selected zone. A robust spatial variation in FRP matched well with corresponding AOD and LST, providing first evidence on possible perturbations of fire on land surface temperature. Hurst exponent reaffirms long-term persistence of fire intensity, surface temperature and aerosol loading time-series. Spatial correlation established a strong temporal association between predictor and dependent variables that too constrained with years. A grid-based analysis over the intensive fire zone concluded a robust increase in LST and AOD during peak fire season.~~

Formatted: Font color: Text 1

The article further employs the Random Forest ~~(RF) ~~model and Geographically w~~W~~eighted r~~R~~egression (GWR) to assess the potential influence of FRP and aerosol loading on LST, while accounting meteorological covariates, physical environment, vegetation characteristic and surface property as confounding factors~~for prevailing meteorological variables~~ within the selected zone. Two contrasting scenarios were hypothesized to examine the FRP–LST–AOD nexus. Scenario 1 considered spatially aggregated FRP from fire initiation to subsidence, whereas Scenario 2 focused on days characterized by high-intensity fires exhibiting a strong positive correlation between FRP and LST. In both the scenarios, the Random Forest ~~RF ~~regression successfully captured and mapped FRP-induced modulation of LST, though with varying magnitudes~~ and model performance~~. A distinct increase in FRP-induced LST modulation was observed during high-intensity fire events. Both boundary layer height and ~~Solar radiation and ~~columnar aerosol loading also contributed partially, with aerosols' influence on LST increasing during periods of intense release of fire energy. The Global Moran's I test indicated significant spatial clustering of LST while GWR results further confirmed FRP and AOD-modulated LST variations across northwestern India, highlighting strong spatial heterogeneity in FRP-AOD-LST nexus.

Formatted: Font color: Text 1

Formatted: Font: Not Bold, Font color: Text 1

Formatted: Font color: Text 1

Formatted: Font: Not Bold, Font color: Text 1

Formatted: Font color: Text 1

Formatted: English (India)

Formatted: Font: 9 pt

This analysis reveals that the biophysical effects of crop residue–based fires across northwestern India can substantially influence the regional radiative budget by altering LST. The magnitude of LST modulation, however, depends on fire intensity and feedbacks from regional meteorology. This study provides novel insights into residue-based fire induced surface temperature dynamics in a region where recurrent fires ha~~s~~ve been historically linked primarily with deteriorating air quality in Delhi and its surroundings. The observation-driven analysis offers a comprehensive understanding of LST responses to residue burning and helps reduce uncertainties in fire-induced modifications of the radiative budget. Nonetheless, uncertainties remain due to unaccounted agricultural feedbacks, limited temporal coverage, retrieval uncertainty in geospatial datasets, and the complexity in aerosol–meteorology interactions. The multifaced influence of fire aerosols and energy on regional climate through rapid atmospheric and land surface adjustments, remains complicated at the global level. Our findings underscore the need for Earth system model–based simulations to better quantify climate feedbacks from crop residue burning. Besides, assessing the underlying mechanisms of fire-energy-induced changes in evapotranspiration, the radiative effects of aerosols, fire–aerosol–meteorology feedbacks, and incorporating additional proxies ~~such as boundary layer height and soil moisture~~ could further reduce the uncertainty in estimating radiative impacts from residue burning.

Formatted: Font: Not Italic, Font color: Auto

Formatted: Font color: Auto, English (India)

~~The article further introduces Random Forest model and Geographically Weighted Regression to ascertain the potential influence of FRP and aerosol loading on LST, taking into account the existing meteorological variables over the selected zone. Two contrasting scenarios were hypothesized to regress the FRP-LST-AOD nexus. Scenario one, considered spatially aggregate FRP from fire initiating days to subside while scenario two accounted for days with very high intensity fire with strong and positive correlation between FRP and LST. Interestingly, for both the cases RF regression was able to capture and map the FRP induced modulation in LST with varying intensities and model performance. A clear increment in FRP induced LST modulation was noted especially during high intensity fire events. Beside FRP, both solar radiation and columnar aerosol loading also noted to partially influence the LST variations although with different intensities. However, the influence of columnar aerosol loading on LST seems to enhance during days with intense energy release possibly linked to excessive emission of carbonaceous aerosols from biomass burning. As Global Moran' I test~~

Formatted: Font: 9 pt

~~concludes significant clustering in LST over the intensive fire zone, the interrelationship between LST and FRP were further assessed using geographically weighted regression. GWR output put further evidences on FRP modulated LST variations over northwest India although it appears to vary strongly with respect to space. Our study therefore, provides a comprehensive insight into the distinctive and persistent LST responses to fire intensity, emphasizing the importance of recognizing the climate feedback from crop residue-based fire dynamics.~~

Acknowledgments

Authors acknowledges the fund received from ~~Climate Change Programme, Department of Science and Technology (DST/CCP/CoE/80/2017-G) and~~ Banaras Hindu University under Institute of Eminence grant (6031). Authors also acknowledge open source software like R (V4.4), Python (V3.7) and QGIS (V3.28) for extracting and plotting the dataset.

Data Availability

~~All the data used in this analysis are available freely. VIIRS and MODIS data can be accessed via NASA Earthdata (https://earthdata.nasa.gov) (last accessed: May 30, 2025), and AgERA5 reanalysis data is available from ECMWF Copernicus (https://cds.climate.copernicus.eu/) (last accessed: May 30, 2025).~~ All the data used in this analysis are available freely. VIIRS and MODIS data can be accessed via NASA Earthdata (https://earthdata.nasa.gov), and ERA5 reanalysis data is available from ECMWF Copernicus (https://cds.climate.copernicus.eu/). SMAP Soil moisture data is available at https://nsidc.org/data/spl1ctb_e. All dataset were last accessed on November 13, 2025. We thank NASA for providing the VIIRS and MODIS data, and the Copernicus Climate Change Service (C3S) for the ERA5 reanalysis data.

~~We thank NASA for providing the VIIRS and MODIS data, and the Copernicus Climate Change Service (C3S) for the AgERA5 reanalysis data.~~

Authors contributions

AP: Data curation, formal analysis and interpretation; RS: Data curation, formal analysis; KA: Data curation, formal analysis; NC: Data curation, formal analysis; TB: conceptualization, methodology and interpretation, funding as well as writing and editing manuscript.

Competing interests. Authors declare that they have no conflict of interest.

Formatted: Font color: Text 1

Formatted: Font color: Text 1

Formatted: Font color: Text 1

Formatted: Font color: Text 1

Formatted: Font color: Text 1

Formatted: Font color: Text 1

Formatted: Font: 9 pt

Supporting Information. The supporting tables (8~~7~~) and figures (~~6~~7~~5~~) are included in supplementary file.

~~Bibliography~~References

Aditi, K., Pandey, A., and Banerjee, T.: Forest fire emission estimates over South Asia using Suomi-NPP VIIRS-based thermal anomalies and emission inventory, Environ. Pollut., 366, 125441, https://doi.org/10.1016/j.envpol.2025.125441, 2025.

Aditi, K., Singh, A., and Banerjee, T.: Retrieval uncertainty and consistency of Suomi-NPP VIIRS Deep Blue and Dark Target aerosol products under diverse aerosol loading scenarios over South Asia, Environ. Pollut., 331, 121913, https://doi.org/10.1016/j.envpol.2023.121913, 2023.

Alkama, R., and Cescatti, A.: Biophysical climate impacts of recent changes in global forest cover, Science, 351, 600–604, https://doi.org/10.1126/science.aac8083, 2016.

Andela, N., Morton, D. C., Giglio, L., Chen, Y., van der Werf, G. R., Kasibhatla, P. S., DeFries, R. S., Collatz, G. J., Hantson, S., Kloster, S., Bachelet, D., Forrest, M., Lasslop, G., Li, F., Mangeon, S., Melton, J. R., Yue, C., and Randerson, J. T.: A human-driven decline in global burned area, Science, 356, 1356–1362, https://doi.org/10.1126/science.aal4108, 2017.

Balwinder-Singh, McDonald, A. J., Srivastava, A. K., Jain, M., and Lobell, D. B.: Trade-offs between groundwater conservation and air pollution from agricultural fires in northwest India, Nat. Sustain., 2, 580–583, https://doi.org/10.1038/s41893-019-0304-4, 2019.

Banerjee, T., Anchule, A., Sorek-Hamer, M., and Latif, M. T.: Vertical stratification of aerosols over South Asian cities, Environ. Pollut., 309, 119776, https://doi.org/10.1016/j.envpol.2022.119776, 2022.

Banerjee, T., Shitole, A. S., Mhawish, A., Anand, A., Ranjan, R., Khan, M. F., Srithawirat, T., Latif, M. T., and Mall, R. K.: Aerosol climatology over South and Southeast Asia: Aerosol types, vertical profile, and source fields, J. Geophys. Res.-Atmos., 126, e2020JD033554, https://doi.org/10.1029/2020JD033554, 2021.

~~Bond, T. C., Doherty, S. J., Fahey, D. W., Forster, P. M., Berntsen, T., DeAngelo, B. J., et al.: Bounding the role of black carbon in the climate system: A scientific assessment, J. Geophys. Res. Atmos., 118, 5380–5552, https://doi.org/10.1002/jgrd.50171, 2013.~~

Bowman, D. M. J. S., Balch, J. K., Artaxo, P., Bond, W. J., Carlson, J. M., Cochrane, M. A., d'Antonio, C. M., DeFries, R. S., Doyle, J. C., Harrison, S. P., Johnston, F. H., Keeley, J. E., Krawchuk, M. A., Kull, C. A., Marston, J. B., Moritz, M. A., Prentice, I. C., Roos, C. I., Scott, A. C., Swetnam, T. W., van der Werf, G. R., and Pyne, S. J.: Fire in the Earth system, Science, 324, 481–484, https://doi.org/10.1126/science.1163886, 2009.

Breiman, L.: Random forests, Mach. Learn., 45, 5–32, https://doi.org/10.1023/A:1010933404324, 2001.

Brunsdon, C., Fotheringham, A. S., and Charlton, M. E.: Geographically weighted regression: A method for exploring spatial nonstationarity, Geogr. Anal., 28, 281–298, https://doi.org/10.1111/j.1538-4632.1996.tb00936.x, 1996.

Brunsdon, C., Fotheringham, S., and Charlton, M.: Geographically weighted regression, J. Roy. Stat. Soc. Ser. D (The Statistician), 47, 431–443, https://doi.org/10.1111/1467-9884.00145, 1998.

Chen, J., Shao, Z., Huang, X., Zhuang, Q., Dang, C., Cai, B., Zheng, X., and Ding, Q.: Assessing the impact of drought–land cover change on global vegetation greenness and productivity, Sci. Total Environ., 852, 158499, https://doi.org/10.1016/j.scitotenv.2022.158499, 2022.

Formatted: Space Before: 6 pt, After: 6 pt, Line spacing: single

Formatted: Font: 9 pt

Chuvieco, E., Pettinari, M. L., Koutsias, N., Forkel, M., Hantson, S., and Turco, M.: Human and climate drivers of global biomass burning variability, Sci. Total Environ., 779, 146361, https://doi.org/10.1016/j.scitotenv.2021.146361, 2021.

Copernicus Climate Change Service: Agrometeorological indicators from 1979 to present derived from reanalysis, Copernicus Climate Change Service (C3S) Climate Data Store (CDS), https://doi.org/10.24381/cds.6c68c9bb, accessed: 25 February 2025, 2020.

Daoud, J. I.: Multicollinearity and regression analysis, J. Phys. Conf. Ser., 949, 012009, https://doi.org/10.1088/1742-6596/949/1/012009, 2017.

~~Eck, T. F., Holben, B. N., Sinyuk, A., Pinker, R. T., Goloub, P., Chen, H., Chatenet, B., Li, Z., Singh, R. P., Tripathi, S. N., and Reid, J. S.: Climatological aspects of the optical properties of fine/coarse mode aerosol mixtures, J. Geophys. Res.-Atmos., 115, D19, https://doi.org/10.1029/2010JD014002, 2010.~~

Fotheringham, A. S., Brunsdon, C., and Charlton, M.: Geographically weighted regression, in: The SAGE Handbook of Spatial Analysis, SAGE Publications, London, 243–254, 2009.

Freychet, N., Tett, S. F. B., Bollasina, M., Wang, K. C., & Hegerl, G.: The local aerosol emission effect on surface shortwave radiation and temperatures. Journal of Advances in Modeling Earth Systems, 11, 806–817. https://doi.org/10.1029/2018MS001530, 2019.

Frazier, P. I.: A tutorial on Bayesian optimization. *arXiv preprint arXiv:1807.02811*, 2018.

Giglio, L., Descloitres, J., Justice, C. O., and Kaufman, Y. J.: An enhanced contextual fire detection algorithm for MODIS, Remote Sens. Environ., 87, 273–282, https://doi.org/10.1016/S0034-4257(03)00184-6, 2003.

Gomez, J. L., Allen, R. J., and Li, K. F.: California wildfire smoke contributes to a positive atmospheric temperature anomaly over the western United States, Atmos. Chem. Phys., 24, 6937–6963, https://doi.org/10.5194/acp-24-6937-2024, 2024.

Graham, M. H.: Confronting multicollinearity in ecological multiple regression, Ecology, 84, 2809–2815, https://doi.org/10.1890/02-3114, 2003.

Granero, M. S., Segovia, J. T., and Pérez, J. G.: Some comments on Hurst exponent and the long memory processes on capital markets, Physica A, 387, 5543–5551, https://doi.org/10.1016/j.physa.2008.05.064, 2008.

Graham, M. H., Haynes, R. J., and Meyer, J. H.: Soil organic matter content and quality: Effects of fertilizer applications, burning, and trash retention on a long-term sugarcane experiment in South Africa, Soil Biol. Biochem., 34, 93–102, https://doi.org/10.1016/S0038-0717(01)00162-2, 2002.

Hurst, H. E.: Long term storage capacity of reservoirs, Trans. Am. Soc. Civ. Eng., 6, 770–799, 1951.

Hsu, N. C., Herman, J. R., and Tsay, S. C.: Radiative impacts from biomass burning in the presence of clouds during boreal spring in Southeast Asia, Geophys. Res. Lett., 30, 1234, https://doi.org/10.1029/2002GL016485, 2003.

Ichoku, C., Giglio, L., Wooster, M. J., and Remer, L. A.: Global characterization of biomass-burning patterns using satellite measurements of fire radiative energy, Remote Sens. Environ., 112, 2950–2962, https://doi.org/10.1016/j.rse.2008.02.009, 2008.

Jacobson, M. Z.: Strong radiative heating due to the mixing state of black carbon in atmospheric aerosols, Nature, 409, 695–697, https://doi.org/10.1038/35055518, 2001.

Jethva, H., Torres, O., Field, R. D., Lyapustin, A., Gautam, R., and Kayetha, V.: Connecting crop productivity, residue fires, and air quality over northern India, Sci. Rep., 9, 16594, https://doi.org/10.1038/s41598-019-52799-x, 2019.

Formatted: Default Paragraph Font, Font: 12 pt, English (India)

Formatted: Space Before: 6 pt, After: 6 pt, Line spacing: single

Formatted: Font: 9 pt

Kant, S., Sarangi, C., and Wilcox, E. M.: Aerosol processes perturb cloud trends over Bay of Bengal: Observational evidence, npj Clim. Atmos. Sci., 6, 132, https://doi.org/10.1038/s41612-023-00442-5, 2023.

Korontzi, S., McCarty, J., Loboda, T., Kumar, S., and Justice, C. O.: Global distribution of agricultural fires in croplands from 3 years of Moderate Resolution Imaging Spectroradiometer (MODIS) data, Glob. Biogeochem. Cycles, 20, GB2021, https://doi.org/10.1029/2005GB002529, 2006.

Lasko, K., and Vadrevu, K.: Improved rice residue burning emissions estimates: Accounting for practice-specific emission factors in air pollution assessments of Vietnam, Environ. Pollut., 236, 795–806, https://doi.org/10.1016/j.envpol.2018.01.114, 2018.

Li, F., Zhang, X., Kondragunta, S., and Csiszar, I.: Comparison of fire radiative power estimates from VIIRS and MODIS observations, J. Geophys. Res.-Atmos., 123, 4545–4563, https://doi.org/10.1029/2017JD027823, 2018.

~~Li, Z., Lau, W. M., Ramanathan, V., Wu, G., Ding, Y., Manoj, M. G., Liu, J., Qian, Y., Li, J., Zhou, T., and Fan, J.: Aerosol and monsoon climate interactions over Asia, Rev. Geophys., 54, 866–929, https://doi.org/10.1002/2015RG000500, 2016.~~

Li, Z. L., Wu, H., Duan, S. B., Zhao, W., Ren, H., Liu, X., Leng, P., Tang, R., Ye, X., Zhu, J., and Sun, Y.: Satellite remote sensing of global land surface temperature: Definition, methods, products, and applications, Rev. Geophys., 61, e2022RG000780, https://doi.org/10.1029/2022RG000780, 2023.

Liu, Z., Ballantyne, A. P., and Cooper, L. A.: Increases in land surface temperature in response to fire in Siberian boreal forests and their attribution to biophysical processes, Geophys. Res. Lett., 45, 6485–6494, https://doi.org/10.1029/2018GL078283, 2018.

Liu, Z., Ballantyne, A. P., and Cooper, L. A.: Biophysical feedback of global forest fires on surface temperature, Nat. Commun., 10, 214, https://doi.org/10.1038/s41467-018-08237-z, 2019.

Logan, T. M., Zaitchik, B., Guikema, S., and Nisbet, A.: Night and day: The influence and relative importance of urban characteristics on remotely sensed land surface temperature, Remote Sens. Environ., 247, 111861, https://doi.org/10.1016/j.rse.2020.111861, 2020.

Lan, R., Eastham, S. D., Liu, T., Norford, L. K., and Barrett, S. R. H.: Air quality impacts of crop residue burning in India and mitigation alternatives, Nat. Commun., 13, 6537, https://doi.org/10.1038/s41467-022-34284-6, 2022.

Markonis, Y., and Koutsoyiannis, D.: Scale-dependence of persistence in precipitation records, Nat. Clim. Change, 6, 399–401, https://doi.org/10.1038/nclimate2894, 2016.

Mhawish, A., Sarangi, C., Babu, P., Kumar, M., Bilal, M., and Qiu, Z.: Observational evidence of elevated smoke layers during crop residue burning season over Delhi: Potential implications on associated heterogeneous PM2.5 enhancements, Remote Sens. Environ., 280, 113167, https://doi.org/10.1016/j.rse.2022.113167, 2022.

NAAS (National Academy of Agricultural Sciences): Innovative viable solution to rice residue burning in rice–wheat cropping system through concurrent use of Super Straw Management System-fitted combines and Turbo Happy Seeder, National Academy of Agricultural Sciences, New Delhi, India, 2017.

Nguyen, H. M., and Wooster, M. J.: Advances in the estimation of high spatio-temporal resolution pan-African top-down biomass burning emissions made using geostationary fire radiative power (FRP) and MAIAC aerosol optical depth (AOD) data, Remote Sens. Environ., 248, 111971, https://doi.org/10.1016/j.rse.2020.111971, 2020.

Prasad, A. K., Singh, R. P., and Kafatos, M.: Influence of coal-based thermal power plants on aerosol optical properties in the Indo-Gangetic Basin, Geophys. Res. Lett., 33, L05805, https://doi.org/10.1029/2005GL023801, 2006.

Formatted: Font: 9 pt

Puissant, A., Rougier, S., & Stumpf, A.: Object-oriented mapping of urban trees using Random Forest classifiers. Int. J. Appl. Earth Obs. Geoinf., 26, 235-245. https://doi.org/10.1016/j.jag.2013.07.002, 2014.

Ramanathan, V., and Carmichael, G.: Global and regional climate changes due to black carbon, Nat. Geosci., 1, 221–227, https://doi.org/10.1038/ngeo156, 2008.

Ramana, M. V., Ramanathan, V., Podgorny, I. A., Pradhan, B. B., and Shrestha, B.: The direct observations of large aerosol radiative forcing due to black carbon in the Himalayan region, Geophys. Res. Lett., 31, L05111, https://doi.org/10.1029/2003GL018824, 2004.

Remer, L. A., Kaufman, Y. J., Tanré, D., Mattoo, S., Chu, D. A., Martins, J. V., Li, R. R., Ichoku, C., Levy, R. C., Kleidman, R. G., Eck, T. F., Vermote, E., and Holben, B. N.: The MODIS aerosol algorithm, products, and validation, J. Atmos. Sci., 62, 947–973, https://doi.org/10.1175/JAS3385.1, 2005.

~~Rosenfeld, D., Zhu, Y., Wang, M., Zheng, Y., Goren, T. and Yu, S.: Aerosol-driven droplet concentrations dominate coverage and water of oceanic low-level clouds. Science, 363(6427), p.eaav0566. https://doi.org/10.1126/science.aav0566, 2019.~~

Sayer, A. M., Hsu, N. C., Bettenhausen, C., and Jeong, M. J.: Validation and uncertainty estimates for MODIS Collection 6 "Deep Blue" aerosol data, J. Geophys. Res.-Atmos., 118, 7864–7872, https://doi.org/10.1002/jgrd.50600, 2013.

Schroeder, W., Oliva, P., Giglio, L., and Csiszar, I. A.: The new VIIRS 375 m active fire detection data product: Algorithm description and initial assessment, Remote Sens. Environ., 143, 85–96, https://doi.org/10.1016/j.rse.2013.12.008, 2014.

Seinfeld, J. H., and Pandis, S. N.: Atmospheric Chemistry and Physics: From Air Pollution to Climate Change, John Wiley & Sons, Hoboken, New Jersey, 2016.

Sharma, N., Kaskaoutis, D. G., Singh, R. P., and Singh, S.: Impact of two intense dust storms and associated mixing with biomass burning aerosols over the Indo-Gangetic Basin, Atmos. Environ., 138, 167–180, https://doi.org/10.1016/j.atmosenv.2016.05.002, 2016.

Shahriari, B., Swersky, K., Wang, Z., Adams, R. P., & De Freitas, N.: Taking the human out of the loop: A review of Bayesian optimization. *Proceedings of the IEEE*, *104*(1), 148-175, 2015.

Shikwambana, L., and Mhangara, P.: Characterization of biomass burning aerosol over southern Africa using multiple satellite data, Int. J. Remote Sens., 39, 4764–4780, https://doi.org/10.1080/01431161.2018.1448481, 2018.

Shikwambana, L., and Mhangara, P.: Analysis of the impact of biomass burning on tropospheric NO2 over southern Africa during 2018, Environ. Pollut., 261, 114204, https://doi.org/10.1016/j.envpol.2020.114204, 2020.

Shikwambana, L., and Kganyago, M.: The contribution of biomass burning to carbon monoxide concentrations in southern Africa: A case study of 2019, Atmosphere, 12, 878, https://doi.org/10.3390/atmos12070878, 2021.

Singh, R. P., and Kaskaoutis, D. G.: Crop residue burning: A threat to South Asian air quality, Eos Trans. AGU, 95, 333–334, https://doi.org/10.1002/2014EO370001, 2014.

Song, C. H., and Carmichael, G. R.: A three-dimensional modeling investigation of the evolution processes of dust and carbonaceous aerosols over East Asia, J. Geophys. Res.-Atmos., 106, 18131–18154, https://doi.org/10.1029/2000JD900511, 2001.

Snoek, J., Larochelle, H., and Adams, R.P.: Practical bayesian optimization of machine learning algorithms. *Advances in neural information processing systems*, *25*, 2012.

Formatted: Space Before: 6 pt, After: 6 pt, Line spacing: single

Formatted: Space Before: 6 pt, After: 6 pt, Line spacing: single

Formatted: Space Before: 6 pt, After: 6 pt, Line spacing: single

Formatted: Font: 9 pt

Srivastava, A. K., Singh, S., Pant, P., Dumka, U. C., and Holben, B. N.: Black carbon aerosols over Manora Peak in the Indian Himalayan foothills: Implications for climate forcing, Environ. Res. Lett., 7, 014002, https://doi.org/10.1088/1748-9326/7/1/014002, 2012.

Stein, A. F., Draxler, R. R., Rolph, G. D., Stunder, B. J. B., Cohen, M. D., and Ngan, F.: NOAA's HYSPLIT atmospheric transport and dispersion modeling system, Bull. Am. Meteorol. Soc., 96, 2059–2077, https://doi.org/10.1175/BAMS-D-14-00110.1, 2015.

Tiwari, S., Singh, A. K., Singh, S., and Pervez, S.: Aerosol climatology over Varanasi using MODIS and MISR satellite data, Air Qual. Atmos. Health, 8, 301–309, https://doi.org/10.1007/s11869-014-0285-8, 2015.

Tian, C., Yue, X., Zhu, J., Liao, H., Yang, Y., Lei, Y., Zhou, X., Zhou, H., Ma, Y., and Cao, Y.: Fire–climate interactions through the aerosol radiative effect in a global chemistry–climate–vegetation model, Atmos. Chem. Phys., 22, 12353–12366, https://doi.org/10.5194/acp-22-12353-2022, 2022.

Vadrevu, K. P., Ellicott, E. A., Giglio, L., Badarinath, K. V. S., Vermote, E., Justice, C., and Lau, W. K. M.: Vegetation fires in the Himalayan region – Aerosol load, black carbon emissions and climate forcing, Remote Sens. Environ., 123, 324–334, https://doi.org/10.1016/j.rse.2012.03.021, 2012.

van der Werf, G. R., Randerson, J. T., Giglio, L., van Leeuwen, T. T., Chen, Y., Rogers, B. M., Mu, M., van Marle, M. J. E., Morton, D. C., Collatz, G. J., Yokelson, R. J., and Kasibhatla, P. S.: Global fire emissions estimates during 1997–2016, Earth Syst. Sci. Data, 9, 697–720, https://doi.org/10.5194/essd-9-697-2017, 2017.

Vadrevu, K. P., Lasko, K., Giglio, L., and Justice, C.: Analysis of Southeast Asian pollution episode using satellite remote sensing data, Atmos. Environ., 125, 512–522, https://doi.org/10.1016/j.atmosenv.2015.11.032, 2016.

Vinjamuri, K.S., Mhawish, A., Banerjee, T., Sorek-Hamer, M., Broday, D.M., Mall, R.K. and Latif, M.T.: Vertical distribution of smoke aerosols over upper Indo-Gangetic Plain. Environmental pollution, 257, p.113377, 2020.

Wang, J., Christopher, S. A., Nair, U. S., Reid, J. S., Prins, E. M., Szykman, J., and Hand, J. L.: Mesoscale modeling of Central American smoke transport to the United States: 1. "Top-down" assessment of emission strength and diurnal variation impacts, J. Geophys. Res.-Atmos., 111, D05S17, https://doi.org/10.1029/2005JD006416, 2006.

Xu, L., Zhu, Q., Riley, W. J., Chen, Y., Wang, H., Ma, P.-L., and Randerson, J. T.: The Influence of Fire Aerosols on Surface Climate and Gross Primary Production in the Energy Exascale Earth System Model (E3SM), J. Climate, 34, 7219–7238, https://doi.org/10.1175/JCLI-D-21-0193.1, 2021.

Yang, J., and Zhao, Y.: Impacts of forest fires on surface temperature and precipitation in boreal regions: An observational analysis, Environ. Res. Lett., 15, 124046, https://doi.org/10.1088/1748-9326/abc123, 2020.

Zhao, T., Li, J., and Zhang, W.: Long-term changes in land surface temperature associated with agricultural burning in eastern China, Remote Sens., 13, 1215, https://doi.org/10.3390/rs13061215, 2021.

~~Aditi K, Pandey A, and Banerjee T (2025): Forest fire emission estimates over South Asia using Suomi-NPP VIIRS-based thermal anomalies and emission inventory,~~ ~~*Environ. Pollut.*~~~~,~~ ~~**366**~~~~, 125441, https://doi.org/10.1016/j.envpol.2025.125441.~~

~~Aditi K, Singh A, and Banerjee T (2023): Retrieval uncertainty and consistency of Suomi-NPP VIIRS Deep Blue and Dark Target aerosol products under diverse aerosol loading scenarios over South Asia,~~ ~~*Environ. Pollut.*~~~~,~~ ~~**331**~~~~, 121913, https://doi.org/10.1016/j.envpol.2023.121913.~~

Formatted: Space Before: 6 pt, After: 6 pt, Line spacing: single

Formatted: Space Before: 6 pt, After: 6 pt, Line spacing: single

Formatted: Space Before: 6 pt, After: 6 pt, Line spacing: single

Formatted: Space Before: 6 pt, After: 6 pt, Line spacing: single

Formatted: Font: 9 pt

~~Alkama R and Cescatti A (2016): Biophysical climate impacts of recent changes in global forest cover, *Science*, **351**, 600–604, https://doi.org/10.1126/science.aac8083.~~

~~Andela N, Morton DC, Giglio L, Chen Y, van der Werf GR, Kasibhatla PS, DeFries RS, Collatz GJ, Hantson S, Kloster S, Bachelet D, Forrest M, Lasslop G, Li F, Mangeon S, Melton JR, Yue C, and Randerson JT (2017): A human-driven decline in global burned area, *Science*, **356**, 1356–1362, https://doi.org/10.1126/science.aal4108.~~

~~Balwinder-Singh, McDonald AJ, Srivastava AK, Jain M, and Lobell DB (2019): Trade-offs between groundwater conservation and air pollution from agricultural fires in northwest India, *Nat. Sustain.*, **2**, 580–583, https://doi.org/10.1038/s41893-019-0304-4.~~

~~Banerjee T, Anchule A, Sorek-Hamer M, and Latif MT (2022): Vertical stratification of aerosols over South Asian cities, *Environ. Pollut.*, **309**, 119776, https://doi.org/10.1016/j.envpol.2022.119776.~~

~~Banerjee T, Shitole AS, Mhawish A, Anand A, Ranjan R, Khan MF, Srithawirat T, Latif MT, and Mall RK (2021): Aerosol climatology over South and Southeast Asia: Aerosol types, vertical profile, and source fields, *J. Geophys. Res.-Atmos.*, **126**, e2020JD033554, https://doi.org/10.1029/2020JD033554.~~

~~Bond TC, Doherty SJ, Fahey DW, Forster PM, Berntsen T, DeAngelo BJ, et al. (2013): Bounding the role of black carbon in the climate system: A scientific assessment, *J. Geophys. Res.-Atmos.*, **118**, 5380–5552, https://doi.org/10.1002/jgrd.50171.~~

~~Bowman DMJS, Balch JK, Artaxo P, Bond WJ, Carlson JM, Cochrane MA, d'Antonio CM, DeFries RS, Doyle JC, Harrison SP, Johnston FH, Keeley JE, Krawchuk MA, Kull CA, Marston JB, Moritz MA, Prentice IC, Roos CI, Scott AC, Swetnam TW, van der Werf GR, and Pyne SJ (2009): Fire in the Earth system, *Science*, **324**, 481–484, https://doi.org/10.1126/science.1163886.~~

~~Breiman L (2001): Random forests, *Mach. Learn.*, **45**, 5–32, https://doi.org/10.1023/A:1010933404324.~~

~~Brunsdon C, Fotheringham AS, and Charlton ME (1996): Geographically weighted regression: A method for exploring spatial nonstationarity, *Geogr. Anal.*, **28**, 281–298, https://doi.org/10.1111/j.1538-4632.1996.tb00936.x.~~

~~Brunsdon C, Fotheringham S, and Charlton M (1998): Geographically weighted regression, *J. Roy. Stat. Soc. Ser. D (The Statistician)*, **47**, 431–443, https://doi.org/10.1111/1467-9884.00145.~~

~~Chen J, Shao Z, Huang X, Zhuang Q, Dang C, Cai B, Zheng X, and Ding Q (2022): Assessing the impact of drought-land cover change on global vegetation greenness and productivity, *Sci. Total Environ.*, **852**, 158499, https://doi.org/10.1016/j.scitotenv.2022.158499.~~

~~Chuvieco E, Pettinari ML, Koutsias N, Forkel M, Hantson S, and Turco M (2021): Human and climate drivers of global biomass burning variability, *Sci. Total Environ.*, **779**, 146361, https://doi.org/10.1016/j.scitotenv.2021.146361.~~

~~Copernicus Climate Change Service (2020): Agrometeorological indicators from 1979 to present derived from reanalysis, *Copernicus Climate Change Service (C3S) Climate Data Store (CDS)*, https://doi.org/10.24381/cds.6c68c9bb (accessed: 25 February 2025).~~

~~Daoud JI (2017): Multicollinearity and regression analysis, *J. Phys. Conf. Ser.*, **949**, 012009, https://doi.org/10.1088/1742-6596/949/1/012009.~~

~~Fotheringham AS, Brunsdon C, and Charlton M (2009): Geographically weighted regression, in: *The SAGE Handbook of Spatial Analysis*, SAGE Publications, London, 243–254.~~

~~Giglio L, Descloitres J, Justice CO, and Kaufman YJ (2003): An enhanced contextual fire detection algorithm for MODIS, *Remote Sens. Environ.*, **87**, 273–282, https://doi.org/10.1016/S0034-4257(03)00184-6.~~

Formatted: Font: 9 pt

~~Gomez JL, Allen RJ, and Li KF (2024): California wildfire smoke contributes to a positive atmospheric temperature anomaly over the western United States, *Atmos. Chem. Phys.*, **24**, 6937–6963, https://doi.org/10.5194/acp-24-6937-2024.~~

~~Graham MH (2003): Confronting multicollinearity in ecological multiple regression, *Ecology*, **84**, 2809–2815, https://doi.org/10.1890/02-3114.~~

~~Graham MH, Haynes RJ, and Meyer JH (2002): Soil organic matter content and quality: Effects of fertilizer applications, burning, and trash retention on a long-term sugarcane experiment in South Africa, *Soil Biol. Biochem.*, **34**, 93–102, https://doi.org/10.1016/S0038-0717(01)00162-2.~~

~~Hurst HE (1951): Long term storage capacity of reservoirs, *Trans. Am. Soc. Civ. Eng.*, **6**, 770–799.~~

~~Hsu NC, Herman JR, and Tsay SC (2003): Radiative impacts from biomass burning in the presence of clouds during boreal spring in Southeast Asia, *Geophys. Res. Lett.*, **30**, 1234, https://doi.org/10.1029/2002GL016485.~~

~~Ichoku C, Giglio L, Wooster MJ, and Remer LA (2008): Global characterization of biomass-burning patterns using satellite measurements of fire radiative energy, *Remote Sens. Environ.*, **112**, 2950–2962, https://doi.org/10.1016/j.rse.2008.02.009.~~

~~Jethva H, Torres O, Field RD, Lyapustin A, Gautam R, and Kayetha V (2019): Connecting crop productivity, residue fires, and air quality over northern India, *Sci. Rep.*, **9**, 16594, https://doi.org/10.1038/s41598-019-52799-x.~~

~~Kant S, Sarangi C, and Wilcox EM (2023): Aerosol processes perturb cloud trends over Bay of Bengal: Observational evidence, *npj Clim. Atmos. Sci.*, **6**, 132, https://doi.org/10.1038/s41612-023-00442-5.~~

~~Korontzi S, McCarty J, Loboda T, Kumar S, and Justice CO (2006): Global distribution of agricultural fires in croplands from 3 years of Moderate Resolution Imaging Spectroradiometer (MODIS) data, *Glob. Biogeochem. Cycles*, **20**, GB2021, https://doi.org/10.1029/2005GB002529.~~

~~Lasko K and Vadrevu K (2018): Improved rice residue burning emissions estimates: Accounting for practice-specific emission factors in air pollution assessments of Vietnam, *Environ. Pollut.*, **236**, 795–806, https://doi.org/10.1016/j.envpol.2018.01.114.~~

~~Li F, Zhang X, Kondragunta S, and Csiszar I (2018): Comparison of fire radiative power estimates from VIIRS and MODIS observations, *J. Geophys. Res.-Atmos.*, **123**, 4545–4563, https://doi.org/10.1029/2017JD027823.~~

~~Li ZL, Wu H, Duan SB, Zhao W, Ren H, Liu X, Leng P, Tang R, Ye X, Zhu J, and Sun Y (2023): Satellite remote sensing of global land surface temperature: Definition, methods, products, and applications, *Rev. Geophys.*, **61**, e2022RG000780, https://doi.org/10.1029/2022RG000780.~~

~~Liu Z, Ballantyne AP, and Cooper LA (2018): Increases in land surface temperature in response to fire in Siberian boreal forests and their attribution to biophysical processes, *Geophys. Res. Lett.*, **45**, 6485–6494, https://doi.org/10.1029/2018GL078283.~~

~~Liu Z, Ballantyne AP, and Cooper LA (2019): Biophysical feedback of global forest fires on surface temperature, *Nat. Commun.*, **10**, 214, https://doi.org/10.1038/s41467-018-08237-z.~~

~~Logan TM, Zaitchik B, Guikema S, and Nisbet A (2020): Night and day: The influence and relative importance of urban characteristics on remotely sensed land surface temperature, *Remote Sens. Environ.*, **247**, 111861, https://doi.org/10.1016/j.rse.2020.111861.~~

~~Lan R, Eastham SD, Liu T, Norford LK, and Barrett SRH (2022): Air quality impacts of crop residue burning in India and mitigation alternatives, *Nat. Commun.*, **13**, 6537, https://doi.org/10.1038/s41467-022-34284-6.~~

Formatted: Font: 9 pt

~~Markonis Y and Koutsoyiannis D (2016): Scale-dependence of persistence in precipitation records, *Nat. Clim. Change*, **6**, 399–401, https://doi.org/10.1038/nclimate2894.~~

~~Mhawish A, Sarangi C, Babu P, Kumar M, Bilal M, and Qiu Z (2022): Observational evidence of elevated smoke layers during crop residue burning season over Delhi: Potential implications on associated heterogeneous $PM_{2.5}$ enhancements, *Remote Sens. Environ.*, **280**, 113167, https://doi.org/10.1016/j.rse.2022.113167.~~

~~NAAS (National Academy of Agricultural Sciences) (2017): *Innovative viable solution to rice residue burning in rice–wheat cropping system through concurrent use of Super Straw Management System-fitted combines and Turbo Happy Seeder*, National Academy of Agricultural Sciences, New Delhi, India.~~

~~Nguyen HM and Wooster MJ (2020): Advances in the estimation of high spatio-temporal resolution pan-African top-down biomass burning emissions made using geostationary fire radiative power (FRP) and MAIAC aerosol optical depth (AOD) data, *Remote Sens. Environ.*, **248**, 111971, https://doi.org/10.1016/j.rse.2020.111971.~~

~~Prasad VK, Gupta PK, Sharma C, Sarkar AK, Kant Y, Badarinath KVS, Rajagopal T, and Mitra AP (2000): NOx emissions from biomass burning of shifting cultivation areas from tropical deciduous forests of India – estimates from ground-based measurements, *Atmos. Environ.*, **34**, 3271–3280, https://doi.org/10.1016/S1352-2310(99)00471-0.~~

~~Peng J, Liu Z, Liu Y, Wu J, and Han Y (2012): Trend analysis of vegetation dynamics in Qinghai–Tibet Plateau using Hurst exponent, *Ecol. Indic.*, **14**, 28–39, https://doi.org/10.1016/j.ecolind.2011.08.010.~~

~~Puissant A, Rougier S, and Stumpf A (2014): Object-oriented mapping of urban trees using Random Forest classifiers, *Int. J. Appl. Earth Obs. Geoinf.*, **26**, 235–245, https://doi.org/10.1016/j.jag.2013.07.002.~~

~~Granero MS, Segovia JT, and Pérez JG (2008): Some comments on Hurst exponent and the long memory processes on capital markets, *Physica A*, **387**, 5543–5551, https://doi.org/10.1016/j.physa.2008.05.064.~~

~~Sarkar S, Singh RP, and Chauhan A (2018): Crop residue burning in northern India: Increasing threat to Greater India, *J. Geophys. Res.-Atmos.*, **123**, 6920–6934, https://doi.org/10.1029/2018JD028428.~~

~~Sayer AM, Hsu NC, Lee J, Kim WV, and Dutcher ST (2019): Validation, stability, and consistency of MODIS Collection 6.1 and VIIRS Version 1 Deep Blue aerosol data over land, *J. Geophys. Res.-Atmos.*, **124**, 4658–4688, https://doi.org/10.1029/2018JD029598.~~

~~Schroeder W, Oliva P, Giglio L, and Csiszar IA (2014): The new VIIRS 375 m active fire detection data product: Algorithm description and initial assessment, *Remote Sens. Environ.*, **143**, 85–96, https://doi.org/10.1016/j.rse.2013.12.008.~~

~~Shyamsundar P, Springer NP, Tallis H, Polasky S, Jat ML, Sidhu HS, Krishnapriya PP, Skiba N, Ginn W, Ahuja V, and Cummins J (2019): Fields on fire: Alternatives to crop residue burning in India, *Science*, **365**, 536–538, https://doi.org/10.1126/science.aaw4085.~~

~~Singh N, Banerjee T, Raju MP, Deboudt K, Sorek-Hamer M, Singh RS, and Mall RK (2018): Aerosol chemistry, transport, and climatic implications during extreme biomass burning emissions over the Indo-Gangetic Plain, *Atmos. Chem. Phys.*, **18**, 14197–14215, https://doi.org/10.5194/acp-18-14197-2018.~~

~~Singh P, Roy A, Bhasin D, Kapoor M, Ravi S, and Dey S (2021): Crop fires and cardiovascular health – a study from North India, *SSM Popul. Health*, **14**, 100757, https://doi.org/10.1016/j.ssmph.2021.100757.~~

Formatted: Font: 9 pt

Singh T, Biswal A, Mor S, Ravindra K, Singh V, and Mor S (2020): A high-resolution emission inventory of air pollutants from primary crop residue burning over Northern India based on VIIRS thermal anomalies, *Environ. Pollut.*, **266**, 115132, https://doi.org/10.1016/j.envpol.2020.115132.

Singh T, Ravindra K, Beig G, and Mor S (2021): Influence of agricultural activities on atmospheric pollution during post-monsoon harvesting seasons at a rural location of Indo-Gangetic Plain, *Sci. Total Environ.*, **796**, 148903, https://doi.org/10.1016/j.scitotenv.2021.148903.

Singh T, Ravindra K, Sreekanth V, Gupta P, Sembhi H, Tripathi SN, and Mor S (2020): Climatological trends in satellite-derived aerosol optical depth over North India and its relationship with crop residue burning: Rural–urban contrast, *Sci. Total Environ.*, **740**, 140963, https://doi.org/10.1016/j.scitotenv.2020.140963.

Streets DG, Yarber KF, Woo JH, and Carmichael GR (2003): Biomass burning in Asia: Annual and seasonal estimates and atmospheric emissions, *Glob. Biogeochem. Cycles*, **17**, 1099, https://doi.org/10.1029/2003GB002040.

Tian C, Yue X, Zhu J, Liao H, Yang Y, Lei Y, Zhou X, Zhou H, Ma Y, and Cao Y (2022): Fire–climate interactions through the aerosol radiative effect in a global chemistry–climate–vegetation model, *Atmos. Chem. Phys.*, **22**, 12353–12366, https://doi.org/10.5194/acp-22-12353-2022.

Vadrevu K and Lasko K (2018): Intercomparison of MODIS Aqua and VIIRS I-band fires and emissions in an agricultural landscape – Implications for air pollution research, *Remote Sens.*, **10**, 978, https://doi.org/10.3390/rs10070978.

Vadrevu KP, Lasko K, Giglio L, Schroeder W, Biswas S, and Justice C (2019): Trends in vegetation fires in South and Southeast Asian countries, *Sci. Rep.*, **9**, 7422, https://doi.org/10.1038/s41598-019-43940-x.

Vinjamuri KS, Mhawish A, Banerjee T, Sorek-Hamer M, Broday DM, Mall RK, and Latif MT (2020): Vertical distribution of smoke aerosols over upper Indo-Gangetic Plain, *Environ. Pollut.*, **257**, 113377, https://doi.org/10.1016/j.envpol.2019.113377.

van der Velde IR, van der Werf GR, Houweling S, Eskes HJ, Veefkind JP, Borsdorff T, and Aben I (2020): Biomass burning combustion efficiency observed from space using measurements of CO and NO_2 by TROPOMI, *Atmos. Chem. Phys. Discuss.*, **2020**, 1–65, https://doi.org/10.5194/acp-2020-403.

Wan Z (2014): New refinements and validation of the Collection-6 MODIS land-surface temperature/emissivity product, *Remote Sens. Environ.*, **140**, 36–45, https://doi.org/10.1016/j.rse.2013.08.027.

Ward DS, Kloster S, Mahowald NM, Rogers BM, Randerson JT, and Hess PG (2012): The changing radiative forcing of fires: Global model estimates for past, present and future, *Atmos. Chem. Phys.*, **12**, 10857–10886, https://doi.org/10.5194/acp-12-10857-2012.

Wang Q, Wang X, Zhou Y, Liu D, and Wang H (2022): The dominant factors and influence of urban characteristics on land surface temperature using random forest algorithm, *Sustain. Cities Soc.*, **79**, 103722, https://doi.org/10.1016/j.scs.2021.103722.

Wooster MJ, Roberts G, Perry GLW, and Kaufman YJ (2005): Retrieval of biomass combustion rates and totals from fire radiative power observations: FRP derivation and calibration relationships between biomass consumption and fire radiative energy release, *J. Geophys. Res. Atmos.*, **110**, D24311, https://doi.org/10.1029/2005JD006318.

Wooster MJ, Zhukov B, and Oertel D (2003): Fire radiative energy for quantitative study of biomass burning: Derivation from the BIRD experimental satellite and comparison to MODIS fire products, *Remote Sens. Environ.*, **86**, 83–107, https://doi.org/10.1016/S0034-4257(03)00070-1.

Formatted: Font: 9 pt

Yang Q, Yuan Q, Yue L, and Li T (2020): Investigation of the spatially varying relationships of $PM_{2.5}$ with meteorology, topography, and emissions over China in 2015 by using modified geographically weighted regression, *Environ. Pollut.*, **262**, 114257, https://doi.org/10.1016/j.envpol.2020.114257.

Yin S (2020): Biomass burning spatiotemporal variations over South and Southeast Asia, *Environ. Int.*, **145**, 106153, https://doi.org/10.1016/j.envint.2020.106153.

Zhang Y, Ge J, Bai X, and Wang S (2025): Blue–green space seasonal influence on land surface temperatures across different urban functional zones: Integrating random forest and geographically weighted regression, *J. Environ. Manage.*, **374**, 123975, https://doi.org/10.1016/j.jenvman.2025.123975.

Zhang W, Yu M, He Q, Wang T, Lin L, Cao K, Huang W, Fu P, and Chen J (2020): The spatial and temporal impact of agricultural crop residual burning on local land surface temperature in three provinces across China from 2015 to 2017, *J. Clean. Prod.*, **275**, 124057, https://doi.org/10.1016/j.jclepro.2020.124057.

Zhao J, Yue C, Wang J, Hantson S, Wang X, He B, Li G, Wang L, Zhao H, and Luyssaert S (2024): Forest fire size amplifies postfire land surface warming, *Nature*, **633**, 828–834, https://doi.org/10.1038/s41586-024-07418-2. Aditi, K., Pandey, A. and Banerjee, T., 2025. Forest fire emission estimates over South Asia using Suomi-NPP VIIRS-based thermal anomalies and emission inventory. Environmental Pollution, 366, p.125441.

Aditi, K., Singh, A. and Banerjee, T., 2023. Retrieval uncertainty and consistency of Suomi-NPP VIIRS Deep Blue and Dark Target aerosol products under diverse aerosol loading scenarios over South Asia. Environmental Pollution, 331, p.121913.

Alkama, R. and Cescatti, A., 2016. Biophysical climate impacts of recent changes in global forest cover. Science, 351(6273), pp.600-604.

Andela, N., Morton, D.C., Giglio, L., Chen, Y., van der Werf, G.R., Kasibhatla, P.S., DeFries, R.S., Collatz, G.J., Hantson, S., Kloster, S. and Bachelet, D., 2017. A human-driven decline in global burned area. *Science*, *356*(6345), pp.1356-1362.

Balwinder-Singh, McDonald, A.J., Srivastava, A.K. *et al.* Tradeoffs between groundwater conservation and air pollution from agricultural fires in northwest India. *Nat Sustain* **2**, 580–583 (2019). https://doi.org/10.1038/s41893-019-0304-4.

Banerjee, T., Anchule, A., Sorek-Hamer, M. and Latif, M.T., 2022. Vertical stratification of aerosols over South Asian cities. Environmental Pollution, 309, p.119776.

Banerjee, T., Shitole, A.S., Mhawish, A., Anand, A., Ranjan, R., Khan, M.F., Srithawirat, T., Latif, M.T. and Mall, R.K., 2021. Aerosol climatology over South and Southeast Asia: Aerosol types, vertical profile, and source fields. Journal of Geophysical Research: Atmospheres, 126(6), p.e2020JD033554.

Bond, T.C., Doherty, S.J., Fahey, D.W., Forster, P.M., Berntsen, T., De Angelo, B.J., et al., 2013. Bounding the role of black carbon in the climate system: a scientific assessment. J. Geophys. Res. 118, 5380e5552.

Bowman, D.M., Balch, J.K., Artaxo, P., Bond, W.J., Carlson, J.M., Cochrane, M.A., d'Antonio, C.M., DeFries, R.S., Doyle, J.C., Harrison, S.P. and Johnston, F.H., 2009. Fire in the Earth system. science, 324(5926), pp.481-484.

Breiman, L. (2001). Random forests. *Machine learning*, *45*, 5-32.

Formatted: Normal (Web), Line spacing: single

Formatted: Font: 9 pt

~~Brunsdon, C., Fotheringham, A.S., Charlton, M.E., 1996. Geographically weighted regression: a method for exploring spatial nonstationarity. Geogr. Anal. 28, 281–298.~~

~~Brunsdon, C., Fotheringham, S., & Charlton, M. (1998). Geographically weighted regression. Journal of the Royal Statistical Society: Series D (The Statistician), 47(3), 431-443.~~

~~Chen, J., Shao, Z., Huang, X., Zhuang, Q., Dang, C., Cai, B., Zheng, X. and Ding, Q., 2022. Assessing the impact of drought-land cover change on global vegetation greenness and productivity. *Science of the Total Environment*, *852*, p.158499.~~

~~Chuvieco, E., Pettinari, M.L., Koutsias, N., Forkel, M., Hantson, S. and Turco, M., 2021. Human and climate drivers of global biomass burning variability. *Science of the Total Environment*, *779*, p.146361.~~

~~Copernicus Climate Change Service (2020). Agrometeorological indicators from 1979 to present derived from reanalysis. Copernicus Climate Change Service (C3S) Climate Data Store (CDS). DOI: 10.24381/cds.6c68c9bb (Accessed on February 25, 2025).~~

~~Daoud, J. I. (2017, December). Multicollinearity and regression analysis. In *journal of physics: Conference series* (Vol. 949, No. 1, p. 012009). IOP Publishing.~~

~~Fotheringham, A. S., Brunsdon, C., & Charlton, M. (2009). Geographically weighted regression. The Sage handbook of spatial analysis, 1, 243-254.~~

~~Giglio, L., Descloitres, J., Justice, C. O., & Kaufman, Y. J. (2003). An enhanced contextual fire detection algorithm for MODIS. Remote Sensing of Environment, 87, 273–282.~~

~~Gomez, J.L., Allen, R.J. and Li, K.F., 2024. California wildfire smoke contributes to a positive atmospheric temperature anomaly over the western United States. Atmospheric Chemistry and Physics, 24(11), pp.6937-6963.~~

~~Graham, M. H. (2003). Confronting multicollinearity in ecological multiple regression. *Ecology*, *84*(11), 2809-2815.~~

~~Graham, M.H., Haynes, R.J. and Meyer, J.H., 2002. Soil organic matter content and quality: effects of fertilizer applications, burning and trash retention on a long-term sugarcane experiment in South Africa. *Soil biology and biochemistry*, *34*(1), pp.93-102.~~

~~Hurst, H., 1951. Long term storage capacity of reservoirs. Trans. Am. Soc. Civil Eng. 6, 770–799.~~

~~Hsu, N.C., Herman, J.R. and Tsay, S.C., 2003. Radiative impacts from biomass burning in the presence of clouds during boreal spring in southeast Asia. Geophysical Research Letters, 30(5).~~

~~Ichoku, C., Giglio, L., Wooster, M.J. and Remer, L.A., 2008. Global characterization of biomass-burning patterns using satellite measurements of fire radiative energy. *Remote sensing of Environment*, *112*(6), pp.2950-2962.~~

~~Jethva, H., Torres, O., Field, R. D., Lyapustin, A., Gautam, R., & Kayetha, V. (2019). Connecting crop productivity, residue fires, and air quality over northern India. *Scientific Reports*, 9(1), 16594.~~

~~Kant, S., Sarangi, C. and Wilcox, E.M., 2023. Aerosol processes perturb cloud trends over Bay of Bengal: observational evidence. *npj Climate and Atmospheric Science*, *6*(1), p.132.~~

Formatted: Font: 9 pt

~~Korontzi, S., McCarty, J., Loboda, T., Kumar, S. and Justice, C.. (2006). Global distribution of agricultural fires in croplands from 3 years of Moderate Resolution Imaging Spectroradiometer (MODIS) data. Global Biogeochemical Cycles, 20(2).~~

~~Lasko, K. and Vadrevu, K., 2018. Improved rice residue burning emissions estimates: Accounting for practice-specific emission factors in air pollution assessments of Vietnam. *Environmental pollution*, *236*, pp.795-806.~~

~~Li, F., Zhang, X., Kondragunta, S., Csiszar, I., 2018. Comparison of fire radiative power estimates from VIIRS and MODIS observations. J. Geophys. Res. Atmos. 123 (9), 4545–4563.~~

~~Li, Z.L., Wu, H., Duan, S.B., Zhao, W., Ren, H., Liu, X., Leng, P., Tang, R., Ye, X., Zhu, J. and Sun, Y., 2023. Satellite remote sensing of global land surface temperature: Definition, methods, products, and applications. *Reviews of Geophysics*, *61*(1).~~

~~Liu, Z., Ballantyne, A. P., & Cooper, L. A. (2018). Increases in land surface temperature in response to fire in Siberian boreal forests and their attribution to biophysical processes. Geophysical Research Letters, 45, 6485–6494. https://doi.org/10.1029/2018GL078283.~~

~~Liu, Z., Ballantyne, A.P. and Cooper, L.A., 2019. Biophysical feedback of global forest fires on surface temperature. *Nature communications*, *10*(1), p.214.~~

~~Logan, T. M., Zaitchik, B., Guikema, S., & Nisbet, A. (2020). Night and day: The influence and relative importance of urban characteristics on remotely sensed land surface temperature. Remote Sensing of Environment, 247, Article 111861.~~

~~Lan, R., Eastham, S.D., Liu, T., Norford, L.K. and Barrett, S.R., 2022. Air quality impacts of crop residue burning in India and mitigation alternatives. Nature communications, 13(1), p.6537.~~

~~Markonis, Y., Koutsoyiannis, D., 2016. Scale-dependence of persistence in precipitation records. Nat. Clim. Chang. 6, 399–401. https://doi.org/10.1038/nclimate2894.~~

~~Mhawish, A., Sarangi, C., Babu, P., Kumar, M., Bilal, M. and Qiu, Z., 2022. Observational evidence of elevated smoke layers during crop residue burning season over Delhi: Potential implications on associated heterogeneous PM2. 5 enhancements. *Remote Sensing of Environment*, *280*, p.113167.~~

~~Markonis, Y., Koutsoyiannis, D., 2016. Scale-dependence of persistence in precipitation records. Nat. Clim. Chang. 6, 399–401. https://doi.org/10.1038/nclimate2894~~

~~Nguyen, H.M. and Wooster, M.J., 2020. Advances in the estimation of high Spatio-temporal resolution pan-African top-down biomass burning emissions made using geostationary fire radiative power (FRP) and MAIAC aerosol optical depth (AOD) data. *Remote Sensing of Environment*, *248*, p.111971.~~

~~Prasad, V.K., Gupta, P.K., Sharma, C., Sarkar, A.K., Kant, Y., Badarinath, K.V.S., Rajagopal, T. and Mitra, A.P., 2000. NOx emissions from biomass burning of shifting cultivation areas from tropical deciduous forests of India–estimates from ground-based measurements. *Atmospheric Environment*, *34*(20), pp.3271-3280.~~

~~Peng, J., Liu, Z., Liu, Y., Wu, J. and Han, Y., 2012. Trend analysis of vegetation dynamics in Qinghai–Tibet Plateau using Hurst Exponent. Ecological Indicators, 14(1), pp.28-39.~~

Formatted: Font: 9 pt

~~Puissant, A., Rougier, S., & Stumpf, A. (2014). Object-oriented mapping of urban trees using Random Forest classifiers. *International Journal of Applied Earth Observation and Geoinformation, 26*, 235-245.~~

~~Ravindra, K., Singh, T., Singh, V., Chintalapati, S., Beig, G. and Mor, S., 2023. Understanding the influence of summer biomass burning on air quality in North India: Eight cities field campaign study. *Science of The Total Environment*, *861*, p.160361.~~

~~Granero, M.S., Segovia, J.T. and Pérez, J.G., 2008. Some comments on Hurst exponent and the long memory processes on capital markets. Physica A: Statistical Mechanics and its applications, 387(22), pp.5543-5551.~~

~~Sarkar, S., Singh, R.P. and Chauhan, A., 2018. Crop residue burning in northern India: Increasing threat to Greater India. *Journal of Geophysical Research: Atmospheres*, *123*(13), pp.6920-6934.~~

~~Sayer, A.M., Hsu, N.C., Lee, J., Kim, W.V., Dutcher, S.T., 2019. Validation, stability, and consistency of MODIS collection 6.1 and VIIRS version 1 deep blue aerosol data over land. J. Geophys. Res. Atmos. 124, 4658–4688~~

~~Schroeder, W., Oliva, P., Giglio, L. and Csiszar, I.A., 2014. The New VIIRS 375 m active fire detection data product: Algorithm description and initial assessment. *Remote Sensing of Environment*, *143*, pp.85-96.~~

~~Shyamsundar, P., Springer, N.P., Tallis, H., Polasky, S., Jat, M.L., Sidhu, H.S., Krishnapriya, P.P., Skiba, N., Ginn, W., Ahuja, V. and Cummins, J., 2019. Fields on fire: Alternatives to crop residue burning in India. *Science*, *365*(6453), pp.536-538.~~

~~Singh, N., Banerjee, T., Raju, M.P., Deboudt, K., Sorek-Hamer, M., Singh, R.S. and Mall, R.K., 2018. Aerosol chemistry, transport, and climatic implications during extreme biomass burning emissions over the Indo-Gangetic Plain. *Atmospheric Chemistry and Physics*, *18*(19), pp.14197-14215.~~

~~Singh, P., Roy, A., Bhasin, D., Kapoor, M., Ravi, S. and Dey, S., 2021. Crop fires and cardiovascular health–a study from North India. *SSM-Population Health*, *14*, p.100757.~~

~~Singh, T., Biswal, A., Mor, S., Ravindra, K., Singh, V. and Mor, S., 2020. A high-resolution emission inventory of air pollutants from primary crop residue burning over Northern India based on VIIRS thermal anomalies. *Environmental Pollution*, *266*, p.115132.~~

~~Singh, T., Ravindra, K., Beig, G. and Mor, S., 2021. Influence of agricultural activities on atmospheric pollution during post-monsoon harvesting seasons at a rural location of Indo-Gangetic Plain. *Science of The Total Environment*, *796*, p.148903.~~

~~Singh, T., Ravindra, K., Sreekanth, V., Gupta, P., Sembhi, H., Tripathi, S.N., Mor, S., 2020. Climatological trends in satellite-derived aerosol optical depth over North India and its relationship with crop residue burning: Rural-urban contrast. Sci. Total Environ. https://doi.org/10.1016/j.scitotenv.2020.140963.~~

~~Streets, D.G., Yarber, K.F.,Woo, J.H., Carmichael, G.R., 2003. Biomass burning in Asia: annual and seasonal estimates and atmospheric emissions. Global Biogeochem. Cycles 17.~~

~~Tian, C., Yue, X., Zhu, J., Liao, H., Yang, Y., Lei, Y., Zhou, X., Zhou, H., Ma, Y. and Cao, Y., 2022. Fire–climate interactions through the aerosol radiative effect in a global chemistry–climate–vegetation model. Atmospheric Chemistry and Physics, 22(18), pp.12353-12366.~~

Formatted: Font: 9 pt

~~Vadrevu, K. and Lasko, K., 2018. Intercomparison of MODIS AQUA and VIIRS I-Band fires and emissions in an agricultural landscape—Implications for air pollution research. *Remote Sensing*, *10*(7), p.978.~~

~~Vinjamuri, K.S., Mhawish, A., Banerjee, T., Sorek-Hamer, M., Broday, D.M., Mall, R.K. and Latif, M.T., 2020. Vertical distribution of smoke aerosols over upper Indo-Gangetic Plain. Environmental pollution, 257, p.113377.~~

~~van Der Velde, I.R., Van Der Werf, G.R., Houweling, S., Eskes, H.J., Veefkind, J.P., Borsdorff, T. and Aben, I., 2020. Biomass burning combustion efficiency observed from space using measurements of CO and NO 2 by TROPOMI. Atmospheric Chemistry and Physics Discussions, 2020, pp.1-65.~~

~~Wan, Z. (2014). New refinements and validation of the collection-6 MODIS land-surface temperature/emissivity product. Remote Sensing of Environment, 140, 36–45. https://doi.org/10.1016/j.rse.2013.08.027~~

~~Ward, D.S., Kloster, S., Mahowald, N.M., Rogers, B.M., Randerson, J.T. and Hess, P.G., 2012. The changing radiative forcing of fires: global model estimates for past, present and future. *Atmospheric Chemistry and Physics*, *12*(22), pp.10857-10886.~~

~~Wang, Q., Wang, X., Zhou, Y., Liu, D. and Wang, H., 2022. The dominant factors and influence of urban characteristics on land surface temperature using random forest algorithm. Sustainable Cities and Society, 79, p.103722.~~

~~Wooster, M.J., Roberts, G., Perry, G.L.W. and Kaufman, Y.J., 2005. Retrieval of biomass combustion rates and totals from fire radiative power observations: FRP derivation and calibration relationships between biomass consumption and fire radiative energy release. *Journal of Geophysical Research: Atmospheres*, *110*(D24).~~

~~Wooster, M.J., Zhukov, B. and Oertel, D., 2003. Fire radiative energy for quantitative study of biomass burning: Derivation from the BIRD experimental satellite and comparison to MODIS fire products. *Remote Sensing of Environment*, *86*(1), pp.83-107.~~

~~Yang, Q., Yuan, Q., Yue, L., & Li, T. (2020). Investigation of the spatially varying relationships of PM2.5 with meteorology, topography, and emissions over China in 2015 by using modified geographically weighted regression. Environmental Pollution, 262(4), 114257.~~

~~Yin, S., 2020. Biomass burning spatiotemporal variations over South and Southeast Asia. *Environment International*, *145*, p.106153.~~

~~Zhang, Y., Ge, J., Bai, X. and Wang, S., 2025. Blue-Green space seasonal influence on land surface temperatures across different urban functional zones: Integrating Random Forest and geographically weighted regression. Journal of Environmental Management, 374, p.123975.~~

~~Zhang, W., Yu, M., He, Q., Wang, T., Lin, L., Cao, K., Huang, W., Fu, P. and Chen, J., 2020. The spatial and temporal impact of agricultural crop residual burning on local land surface temperature in three provinces across China from 2015 to 2017. Journal of Cleaner Production, 275, p.124057.~~

~~Zhao, J., Yue, C., Wang, J., Hantson, S., Wang, X., He, B., Li, G., Wang, L., Zhao, H. and Luyssaert, S., 2024. Forest fire size amplifies postfire land surface warming. Nature, 633(8031), pp.828-834.~~

Formatted: Normal (Web)

Formatted: Font: 9 pt